

1           **Characterization of the *Chlamydomonas reinhardtii* phycosphere reveals conserved**  
2           **features of the plant microbiota**

3  
4 Paloma Durán<sup>1,2,†</sup>, José Flores-Uribe<sup>1,†</sup>, Kathrin Wippel<sup>1</sup>, Pengfan Zhang<sup>1</sup>, Rui Guan<sup>1</sup>, Ruben  
5 Garrido-Oter<sup>1,2,+</sup>

6  
7 <sup>1</sup> Department of Plant-Microbe Interactions, Max Planck Institute for Plant Breeding Research,  
8 50829 Cologne, Germany.

9 <sup>2</sup> Cluster of Excellence on Plant Sciences, 40225 Düsseldorf, Germany.

10 † Co-first authors

11 + Correspondence to: [garridoo@mpipz.mpg.de](mailto:garridoo@mpipz.mpg.de)

12

13 **Abstract**

14 Microscopic algae release organic compounds to the region immediately surrounding their cells,  
15 known as the phycosphere, constituting a niche for colonization by heterotrophic bacteria. These  
16 bacteria take up algal photoassimilates and provide beneficial functions to their host, in a process  
17 that resembles the establishment of microbial communities associated with the roots and  
18 rhizospheres of land plants. Here, we characterize the microbiota of the model alga  
19 *Chlamydomonas reinhardtii* and reveal extensive taxonomic and functional overlap with the root  
20 microbiota of land plants. Reconstitution experiments using synthetic communities derived from  
21 *C. reinhardtii* and *Arabidopsis thaliana* show that phycosphere and root bacteria assemble into  
22 taxonomically equivalent communities on either host. We show that provision of diffusible  
23 metabolites is not sufficient for phycosphere community establishment, which additionally requires  
24 physical proximity to the host. Our data suggests that the microbiota of photosynthetic organisms,  
25 including green algae and flowering plants, assembles according to core ecological principles.

## 26 Introduction

27 Plants associate with diverse microbes in their aerial and belowground tissues which are recruited  
28 from the surrounding environment. These microbial communities, known as the plant microbiota,  
29 provide the host with beneficial functions, such as alleviation of abiotic stresses (Xu *et al.*, 2018;  
30 Berens *et al.*, 2019; Simmons *et al.*, 2020; Zélicourt *et al.*, 2018), nutrient mobilization (Castrillo *et al.*,  
31 2017; Zhang *et al.*, 2019; Harbort *et al.*, 2020), or protection against pathogens (Durán *et al.*,  
32 2018; Carrión *et al.*, 2019). Characterization of the microbiota associated with a wide range of  
33 plant species including liverworts (Alcaraz *et al.*, 2018), lycopods, ferns (Yeoh *et al.*, 2017),  
34 gymnosperms (Beckers *et al.*, 2017; Cregger *et al.*, 2018), and angiosperms (Bulgarelli *et al.*,  
35 2012; Lundberg *et al.*, 2012; Edwards *et al.*, 2015; Schlaeppli *et al.*, 2014; Bulgarelli *et al.*, 2015;  
36 Zgadżaj *et al.*, 2016; Walters *et al.*, 2018; Thiergart *et al.*, 2020) shows a strong influence of host  
37 phylogeny as well as conserved and possibly ancestral community features. Furthermore, it has  
38 been speculated that the ability to form associations with members of these communities, such as  
39 mycorrhizal fungi, was a trait required for the colonization of land by plants 450 Mya, possibly  
40 inherited from their algal ancestor (Delaux *et al.*, 2015; Knack *et al.*, 2015). Algae are also known  
41 to associate with complex bacterial communities termed phycosphere microbiota, particularly in  
42 aquatic environments (Kim *et al.*, 2014; Amin *et al.*, 2015; Seymour *et al.*, 2017; Cirri *et al.*, 2019),  
43 where exchange of metabolites, including organic carbon (Moran *et al.*, 2016; Wienhausen *et al.*,  
44 2017; Fu *et al.*, 2020; Toyama *et al.*, 2018), soluble micronutrients (Amin *et al.*, 2009), vitamins  
45 (Croft *et al.*, 2005; Grant *et al.*, 2014; Paerl *et al.*, 2017), and other molecular currencies (Teplitski  
46 *et al.*, 2004; Wichard *et al.*, 2015) influence algal growth and development. These parallelisms  
47 suggest that the phycosphere is analogous to the rhizosphere environment, in which secreted  
48 diffusible compounds alter soil pH, oxygen availability, concentration of antimicrobials and organic  
49 carbon, and thus support distinct microbial communities by favoring the growth of certain bacteria  
50 while restricting proliferation of others (Bell and Mitchell, 1972; Bulgarelli *et al.*, 2013; Amin *et al.*,  
51 2015; Krohn-Molt *et al.*, 2017; Shibl *et al.*, 2020). However, it is not yet known whether the ability  
52 to assemble a complex microbiota from the surrounding soil is also conserved in soil-borne  
53 microscopic algae, and to what extent they overlap with those of vascular plants.

54 In this study, we characterize the microbiota of the model green alga *C. reinhardtii* (*Cr*), and show  
55 significant taxonomic and functional similarities between the root and phycosphere microbiota. In  
56 addition, we report a comprehensive, whole-genome sequenced culture collection of *Cr*-  
57 associated bacteria that includes representatives of the major taxa found in associations with land  
58 plants. We then introduce a series of gnotobiotic systems designed to reconstruct artificial  
59 phycospheres that recapitulate natural communities using synthetic communities (SynComs)

60 assembled from bacterial isolates. Cross-inoculation and competition experiments using the  
61 model plant *Arabidopsis thaliana* (*At*) and its associated bacterial culture collection (Bai *et al.*,  
62 2015) indicate a degree of functional equivalence between phycosphere and root bacteria in  
63 associations with a photosynthetic host. Finally, we show that physical proximity between *Cr* and  
64 its microbiota is required for the establishment of fully functional phycosphere communities,  
65 suggesting that this process is not exclusively driven by the exchange of diffusible metabolites.

## 66 Results

### 67 *C. reinhardtii* assembles a distinct microbiota from the surrounding soil

68 To determine whether *Cr* shapes soil-derived bacterial communities similarly to land plants, we  
69 designed an experiment where *At* and *Cr* were grown in parallel in natural soil in the greenhouse  
70 (Fig. S1A). Briefly, pots containing Cologne Agricultural Soil (CAS) were inoculated with axenic  
71 *Cr* (CC1690) cultures or sowed with surface-sterilized *At* (Col-0) seeds. We then collected  
72 samples from unplanted controls and from the surface of *Cr*-inoculated pots (phycosphere  
73 fraction) at 7-day intervals, and harvested the root and rhizosphere of *At* plants after 36 days  
74 (Methods). Bacterial communities from all compartments were characterized by 16S rRNA  
75 amplicon sequencing. Analysis of bacterial community profiles showed a decrease in  $\alpha$ -diversity  
76 (Shannon index) in the phycosphere and root compartments compared to the more complex soil  
77 and rhizosphere communities (Fig. 1A). In addition, analysis of  $\beta$ -diversity revealed a significant  
78 separation by compartment, where phycosphere and root samples formed distinct clusters that  
79 were also separated from those consisting of soil and rhizosphere samples (Fig. 1B; 22.4% of  
80 variance;  $P < 0.001$ ). Further inspection of amplicon profiles showed an overlap between root- and  
81 phycosphere-associated communities along the second and third components (Fig. 1C),  
82 suggesting similarities between the bacterial communities that associate with *Cr* phycospheres  
83 and *At* roots.

84 To characterize the dynamics of these microbiota assembly processes, we analyzed the time-  
85 series data from soil and phycosphere and end-point community profiles from *At* roots. This  
86 revealed a gradual recruitment of bacterial taxa from soil, leading to the formation of distinct  
87 phycosphere communities that become significantly differentiated 21 days after inoculation, which  
88 is of comparable to that observed in *At* root-associated communities at day 36 (Fig. S2A).  
89 Subsequent enrichment analysis of amplicon sequence variants (ASVs) in each compartment,  
90 compared to unplanted soil, showed an increase in the relative abundance of *Cr*- and *At*-enriched  
91 ASVs in phycosphere and root samples, respectively. In contrast, total relative abundance of soil-  
92 enriched ASVs progressively decreased in host-associated compartments, while remaining stable

93 in unplanted soil (**Fig. S2B-D**). Although the magnitude of the changes in bacterial community  
94 composition in the phycosphere diminishes over time, it remains unclear whether these  
95 communities reach a steady state over the duration of the experiment. Taken together, these  
96 results indicate that, similarly to *At*, *Cr* is able to recruit a subset of bacterial taxa from the  
97 surrounding soil and assemble a distinct microbiota.

### 98 **The *C. reinhardtii* phycosphere and the plant root share a core microbiota**

99 Given the observed similarities between phycosphere and root communities (**Fig. 1C**), we  
100 compared the most abundant taxonomic groups found in association with the two photosynthetic  
101 hosts. We found a significant overlap between Operational Taxonomic Units (OTUs) with the  
102 highest relative abundances in either phycosphere or root samples (**Fig. 1D**; >0.1% relative  
103 abundance; 32% shared;  $P < 0.001$ ), which included members of every bacterial order except  
104 Myxococcales, which were only found in large relative abundances in *At* root samples  
105 (**Supplementary Data 1**). In line with previous descriptions of the *At* root microbiota, we observed  
106 that these host-associated communities were dominated by Proteobacteria, and also included  
107 members of the Actinobacteria, Bacteroidetes, and Firmicutes phyla. At this taxonomic level, the  
108 major difference between the two photosynthetic hosts was given by a lower contribution of  
109 Actinobacteria and a larger relative abundance of Firmicutes in the *Cr* phycosphere compared to  
110 the *At* root compartment (**Fig. 1D**). Given that this latter phylum is most abundant in soil, this  
111 difference may be due to the difficulty of fully separating soil particles from the phycosphere  
112 fraction during sample collection.

113 Next, we sought to assess whether the observed overlap in community structures between *Cr* and  
114 *At* could be extended to other land plant lineages. We performed a meta-analysis, broadening our  
115 study to include samples from phylogenetically diverse plant species found in a natural site,  
116 including lycopods, ferns, gymnosperms, and angiosperms (Yeoh *et al.*, 2017), as well as the  
117 model legume *Lotus japonicus* (*Lj*) grown in CAS soil in the greenhouse (Thiergart *et al.*, 2019;  
118 Harbort *et al.*, 2020). First, we determined which taxonomic groups were present in each plant  
119 species ( $\geq 80\%$  occupancy and  $\geq 0.1\%$  average relative abundance) and identified a total of six  
120 bacterial orders that consistently colonize plant roots (i.e., found in every host species). These  
121 taxa include Caulobacteriales, Rhizobiales, Sphingomonadales, Burkholderiales,  
122 Xanthomonadales (Proteobacteria), and Chitinophagales (Bacteroidetes). We observed that the  
123 aggregated relative abundance of these six bacterial orders accounted for 39% of their respective  
124 communities on average (**Fig. 2**). Interestingly, these taxa were also found among the most  
125 abundant in the *Cr* phycosphere (45% aggregated relative abundance), indicating that they are  
126 also able to associate with *Cr*. These results suggest the existence of a common principle for

127 microbiota assembly across a wide phylogenetic range of photosynthetic hosts, which includes  
128 uni- and multicellular eukaryotic organisms.

### 129 **Reconstitution of phycosphere communities using reductionist approaches**

130 After the characterization of phycosphere-associated bacterial communities in natural soil, we  
131 sought to develop systems of reduced complexity that would allow controlled perturbation of  
132 environmental parameters, and targeted manipulation of microbial community composition. First,  
133 we established a mesocosm system using soil-derived microbial communities as start inocula  
134 (**Fig. S1B**). We co-inoculated axenic *Cr* (CC1690) cultures with microbial extracts from two soil  
135 types (CAS and Galm) in two different carbon-free media (TP and B&D), which ensures that the  
136 only source of organic carbon to sustain bacterial growth is derived from *Cr* photosynthetic activity  
137 (**Methods**). These phycosphere mesocosms were then incubated under continuous light for 11  
138 days, during which we assessed *Cr* growth using cell counts, and profiled bacterial communities  
139 via 16S rRNA amplicon sequencing. In this system, *Cr* was able to steadily grow without a  
140 detrimental impact from co-inoculation with soil-derived bacterial extracts (**Fig. S3A**). Analysis of  
141 diversity showed that *Cr* was able to shape soil-derived bacterial communities within the first 4  
142 days, compared to the starting inocula, and that these phycosphere communities remained stable  
143 until the end of the experiment (**Fig. 3**). Interestingly, cultivation of soil-derived bacteria in the  
144 absence of organic carbon or supplemented with Artificial Photosynthates (AP; **Methods**) led to  
145 significantly differentiated bacterial communities (**Fig. 3A**; 17.9% of variance;  $P < 0.001$ ). In  
146 addition, inoculation of soil-derived bacteria with heat-killed *Cr* cultures was not sufficient to  
147 recapitulate this community shift (**Fig. S3B**), suggesting that the presence of live and metabolically  
148 active *Cr* is required for the establishment of synthetic phycospheres. We then tested whether  
149 larger eukaryotic microorganisms present in the soil microbial extracts, such as other unicellular  
150 algae or fungi, were also contributing to the observed changes in bacterial composition. A separate  
151 experiment, where microbial inocula were filtered through a 5  $\mu\text{m}$  pore-size membrane, showed  
152 similar bacterial community shifts compared to non-filtered extracts (**Fig. S3C**). Similar to the  
153 results obtained using natural soil, the aggregated relative abundance of *Cr*-associated ASVs in  
154 the synthetic phycosphere samples increased over time, whereas ASVs enriched in the bacteria  
155 only control samples consistently decreased (**Fig. 3B**). At the end of the experiment (day 11), the  
156 relative abundance of *Cr*-enriched ASVs accounted for 94% of the entire phycosphere community,  
157 in contrast to a lower contribution observed in the natural soil system (**Fig. S2B**; 60% relative  
158 abundance at day 36). This pattern could be a consequence of the unintended depletion of  
159 bacteria that are not capable of metabolizing *Cr*-secreted photoassimilates in a liquid environment,  
160 and in these specific culture media. Finally, an independent mesocosm experiment using day/night

161 light cycles showed delayed but similar patterns to those using continuous light, indicating that  
162 phycosphere community establishment may be independent of *Cr* culture synchronization (**Fig.**  
163 **S3D**).

164 Next, we aimed to control community composition in this reductionist system by establishing a *Cr*-  
165 associated bacterial culture collection following a similar approach as reported in previous studies  
166 with land plants ([Bai et al., 2015](#); [Lebeis et al., 2015](#); [Eida et al., 2018](#); [Garrido-Oter et al., 2018](#);  
167 [Wippel et al., 2021](#); [Zhang et al., 2021a](#)). We employed a limiting dilution approach using 7 day-  
168 old *Cr* phycospheres derived from CAS soil bacteria incubated in two minimal media (TP and B&D;  
169 **Methods**). The resulting sequence-indexed phycosphere bacterial library (*Cr*-IPL) contained a  
170 total of 1,645 colony forming units (CFUs), which were taxonomically characterized by 16S rRNA  
171 amplicon sequencing. Comparison of these sequencing data with the community profiling of soil  
172 phycospheres revealed that we were able to recover 62% of the most abundant bacterial OTUs  
173 found in natural communities (**Fig. S4A**; **Supplementary Data 2**). Recovered OTUs accounted  
174 for up to 63% of the cumulative relative abundance of the entire culture-independent community,  
175 indicating that our collection is taxonomically representative of *Cr* phycosphere microbiota. These  
176 results are comparable to the recovery rates observed in previously reported culture collections  
177 from different plant species (e.g., 57% for *A. thaliana*, [Bai et al., 2015](#); 69% for rice, [Zhang et al.,](#)  
178 [2019](#); 53% for *L. japonicus*; [Wippel et al., 2021](#)).

179 To establish a core collection of phycosphere bacteria, we selected a taxonomically representative  
180 set of strains from the *Cr*-IPL covering all major taxonomic groups found in the culture-independent  
181 community profiles and subjected them to whole-genome sequencing (**Methods**). In total, we  
182 sequenced the genomes of 185 bacterial isolates, classified into 42 phylogroups (97% average  
183 nucleotide identity), belonging to 5 phyla and 15 families (**Supplementary Data 3**). Next, we  
184 performed comparative analyses of the genomes from the phycosphere core collection (*Cr*-  
185 SPHERE) with those established from soil, roots of *A. thaliana*, and roots and nodules of *L.*  
186 *japonicus* (*At*- and *Lj*-SPHERE) grown in the same soil (CAS). A whole-genome phylogeny of  
187 these bacterial strains showed that all major taxonomic groups that included root-derived isolates  
188 were also represented in the *Cr*-SPHERE collection, but not in the soil collection (**Fig. S4B**).  
189 Importantly, the phycosphere collection also included multiple representatives of each of the six  
190 bacterial orders that were found to consistently colonize plant roots in natural environments (**Fig.**  
191 **2**). Next, we assessed the functional potential encoded in the genomes of the sequenced  
192 phycosphere bacteria using the KEGG orthology database as a reference ([Kanehisa et al., 2014](#)).  
193 Principal coordinates analysis (PCoA) of functional distances showed that bacterial taxonomy



194 accounted for most of the variance of the data (58.63%;  $P < 0.001$ ), compared to a much smaller  
195 impact of the host of origin of the genomes (4.22% of variance;  $P < 0.001$ ; **Fig S4C**).

196 Next, we tested whether synthetic communities formed by isolates from the *Cr*-SPHERE collection  
197 could recapitulate assembly patterns of natural phycospheres under laboratory conditions. Axenic  
198 *Cr* cultures (CC1690) were inoculated with a bacterial SynCom composed of 26 strains that could  
199 be distinguished at the 16S level and contained representative members of all major phycosphere  
200 taxonomic groups (**Fig. S1D**; **Supplementary Data 4**). Assessment of *Cr* growth using chlorophyll  
201 fluorescence and cell counts showed that the presence of the bacterial SynCom had no consistent  
202 beneficial or detrimental impact on *Cr* proliferation in this system (**Fig. 4A-B**), similarly to what we  
203 observed in mesocosms (**Fig. S3A**). Analysis of time-course amplicon profiles showed that *Cr*  
204 assembled a characteristic phycosphere community within the first 4 days of co-inoculation, which  
205 was significantly separated from both, start inocula and bacterial SynComs alone (**Fig. 4C-D**).  
206 Together, these results demonstrate that we can recapitulate *Cr* assembly of distinct phycosphere  
207 communities in natural soils using culture-dependent and -independent gnotobiotic systems.

#### 208 ***Cr*- and *At*-derived SynComs form taxonomically equivalent communities on either host**

209 Given the similarity between phycosphere and root communities observed in natural soils (**Fig. 1**),  
210 and the taxonomic and functional overlap across genomes from their corresponding core  
211 collections (**Fig. S4B-C**), we hypothesized that SynComs with the same taxonomic composition  
212 would assemble into similar communities, regardless of their origin. To test this hypothesis, we  
213 used a soil-based gnotobiotic system in which we could grow *Cr* and *At* in parallel, in addition to  
214 the previously described liquid-based system (**Methods**). We designed taxonomically-paired  
215 SynComs composed of strains from either the IPL (*Cr*-SPHERE) or IRL (*At*-SPHERE) bacterial  
216 culture collections. In these SynComs we included one representative strain from each bacterial  
217 family shared between the two collections ( $n=9$ ), ensuring that they could be differentiated by their  
218 16S rRNA sequences (**Supplementary Data 4**). We then inoculated axenic *Cr* cultures and *At*  
219 seeds with either IPL, IRL or mixed (IPL+IRL) SynComs and allowed to colonize either host for  
220 four weeks (**Fig. S1E**). Next, we harvested the root, soil, and phycosphere fractions, measured  
221 host growth, and performed 16S rRNA amplicon sequencing (**Methods**). Assessment of growth  
222 parameters (cell counts for bacteria and *Cr*, chlorophyll content for *Cr* and shoot fresh weight for  
223 *At*) showed no significant differences across SynCom treatments (**Fig. S5**). However, analysis of  
224 community profiles of the mixed SynComs showed that *Cr* and *At* assemble distinct communities  
225 that could also be clearly separated from unplanted soil (**Fig. 5A**). Similar to what we observed in  
226 natural soil (**Fig. 1C**), there was an overlap between phycosphere and root samples, which  
227 clustered together along the second and third components (**Fig. 5B**). Interestingly, analysis of

228 community composition at the family level showed that all SynComs (*Cr*-, *At*-derived, and mixed)  
229 formed taxonomically indistinguishable root or phycosphere communities, independently of their  
230 host of origin (**Fig. 5A-B**). Furthermore, analysis of aggregated relative abundances from mixed  
231 communities showed that phycosphere-derived strains could successfully colonize *At* roots  
232 (48.32% relative abundance), and root-derived strains established associations with *Cr* in both  
233 soil and liquid systems (42.94% and 25.70% relative abundance, respectively; **Fig. 5C-D**). Despite  
234 this capacity for ectopic colonization, we observed significant signatures of host preference in  
235 SynComs from the two culture collections, indicated by the fact that *Cr*-derived strains reached  
236 higher aggregated relative abundances in the phycosphere compared to the root, while the  
237 opposite pattern was identified for *At*-derived bacteria (**Fig. 5C**). This tendency was accentuated  
238 in the liquid system, where *Cr* bacteria outcompeted *At* strains in the presence of the algae but  
239 not when they were incubated alone (**Fig. 5D**). Taken together, these results suggest the presence  
240 of conserved features in bacterial members of the *Cr* and *At* microbiota at a high taxonomic level,  
241 with signatures of host preference at the strain level.

#### 242 **Physical proximity is required for the assembly of phycosphere communities and** 243 **promotion of *Cr* growth**

244 Next, we sought to investigate whether the observed formation of distinct phycosphere  
245 communities (**Figs. 1, 3 and 4**) is driven by the secretion of diffusible photoassimilates and to what  
246 extent physical proximity to bacteria is required to establish other forms of interactions. To test  
247 this hypothesis, we developed a gnotobiotic split co-cultivation system where synthetic  
248 phycospheres could be grown photoautotrophically (**Fig. S1F**). In this system, two growth  
249 chambers were connected through a 0.22  $\mu\text{m}$ -pore polyvinylidene fluoride (PVDF) membrane that  
250 allows diffusion of compounds but not passage of bacterial or algal cells (**Methods**). We co-  
251 cultivated axenic *Cr* cultures (C), bacterial SynComs (SC), and synthetic phycospheres (C+SC) in  
252 these split chambers containing minimal carbon-free media (TP) in multiple pair-wise  
253 combinations (**Fig. S1F**; **Supplementary Data 4**). Analysis of 16S rRNA amplicon profiles after 7  
254 days of incubation revealed that SC and C+SC samples were distinguishable from the input  
255 bacterial SynComs (**Fig. 6A**). In addition, samples clustered according to the presence of *Cr* in  
256 the same compartment, causing SC and C+SC samples to be significantly separated,  
257 independently of the community present in the neighboring chamber (**Fig. 6A**, indicated by colors;  
258 21.4% of variance;  $P < 0.001$ ). Comparison of amplicon profiles of samples taken from chambers  
259 containing C+SC further showed a significant impact of the content of the neighboring  
260 compartment in community structures (**Fig. 6B**, indicated by shapes; 39.5% of variance;  $P < 0.001$ ).  
261 Interestingly, we also observed that the presence of *Cr* in the neighboring compartment was



262 sufficient to change SC communities where the bacterial SynCom was incubated alone (**Fig. 6C**;  
263 **SC|C** or **SC|C+SC** *versus* **SC|–**;  $P=0.001$ ), possibly by secreting diffusible compounds or inducing  
264 changes in the composition of the culture medium (e.g., minerals, pH). Furthermore, SC  
265 communities where *Cr* was present in the neighboring compartment could be differentiated  
266 depending on whether *Cr* was in direct contact with bacteria or grown axenically (**Fig. 6C**; **SC|C**  
267 *versus* **SC|C+SC**). These community shifts could be explained by competition for diffusible  
268 metabolites with the neighboring compartment containing the SynCom together with the algae  
269 (C+SC), or by physiological changes in *Cr* induced by physical proximity with bacteria.

270 In parallel to bacterial community profiles, we assessed *Cr* growth by measuring chlorophyll  
271 fluorescence and algal cell counts in all vessels (**Methods**). We observed significant differences  
272 in the growth of axenic *Cr* cultures depending on the contents of the neighboring chamber, where  
273 the bacterial SynCom alone (**C|SC**) had a positive impact on the microalgae compared to the  
274 control (**C|–**; **Fig. 6D-E**). Remarkably, the presence of a synthetic phycosphere in the neighboring  
275 compartment had the strongest positive impact on axenic *Cr* cultures (**C|C+SC**; **Fig. 6D-E**),  
276 suggesting that changes in bacterial community composition driven by physical proximity to *Cr*  
277 lead to a beneficial impact on algal growth. In addition, chlorophyll fluorescence and cell counts of  
278 synthetic phycospheres (C+SC) were higher when no other microorganisms were incubated in the  
279 neighboring chamber (**C+SC|–** *versus* **C+SC|C** or **C+SC|SC**; **Fig. 6D-E**), possibly due to  
280 competition for diffusible compounds. An additional full-factorial replicate experiment using a  
281 modified version of this split co-cultivation system (**Methods**) showed consistent results both in  
282 community structures and *Cr* growth parameters (**Fig. S6**), despite of a large technical variation  
283 in cell density measurements (**Fig. 6D**). Together, these results indicate that physical proximity of  
284 bacteria to *Cr* is required for assembly and growth of phycosphere communities, which in turn may  
285 benefit host growth by providing metabolites and / or other compounds including carbon dioxide,  
286 which in this experimental setup is likely limiting autotrophic growth of *Cr*. Future experimentation  
287 with synthetic phycospheres composed by SynComs designed using combinatorial approaches,  
288 coupled with metabolomic and transcriptomic profiling, will be needed to decipher the molecular  
289 and genetic mechanisms driving these interactions.

## 290 **Discussion**

291 Microscopic algae release photoassimilated carbon to the diffusible layer immediately surrounding  
292 their cells, which constitutes a niche for heterotrophic bacteria. Microbes from the surrounding  
293 environment compete for colonization of this niche and assemble into complex communities that  
294 play important roles in global carbon and nutrient fluxes. These ecological interactions have been  
295 well studied in aquatic environments, where each year approximately 20 Gt of organic carbon

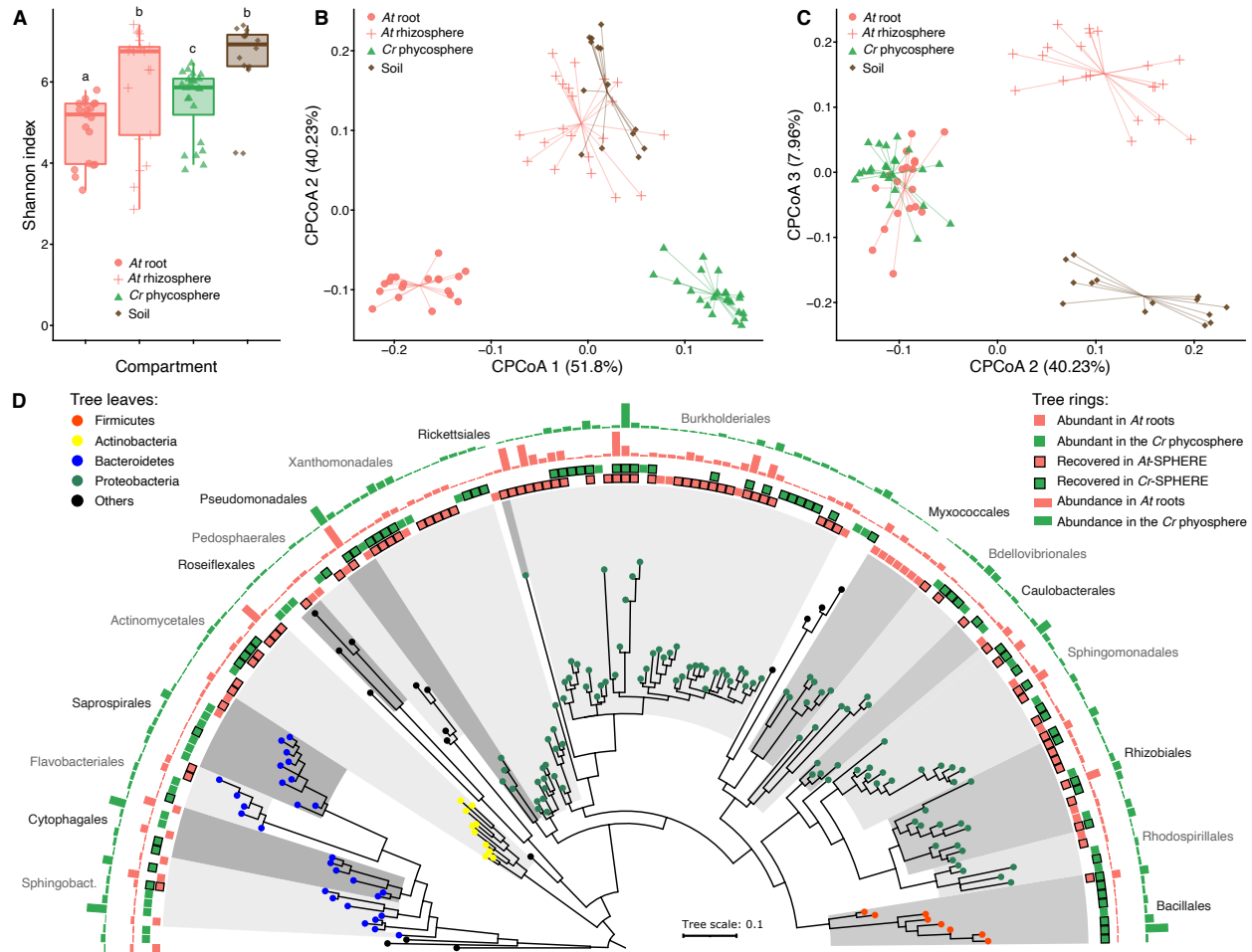
296 fixed by phytoplankton are taken up by heterotrophic bacteria (Moran *et al.*, 2016), which can  
297 account for up to 82% of all algal-derived organic matter (Horňák *et al.*, 2017). For multiple species  
298 of green algae, optimal growth in turn requires interactions with their associated phycosphere  
299 bacteria, which can provide beneficial services to their host, such as mobilization of non-soluble  
300 iron (Amin *et al.*, 2009), or exogenous biosynthesis of organic compounds such as vitamins (Croft  
301 *et al.*, 2005; Paerl *et al.*, 2017). Despite the known importance of these interactions in marine  
302 environments, the role of algae-bacterial associations in terrestrial ecosystems remains  
303 understudied. This gap in our understanding could be explained by the fact that aquatic  
304 phytoplankton are more readily noticed and more amenable to systematic study compared to  
305 edaphic microalgae. However, exploring the role of soil-borne unicellular photosynthetic  
306 organisms as hosts of complex microbial communities could expand our understanding of carbon  
307 and energy fluxes in terrestrial ecosystems.

308 The results from our culture-independent and gnotobiotic experiments using the ubiquitous algae  
309 *Cr*, which was originally isolated from soil (Sasso *et al.*, 2018), illustrate that green algae can  
310 recruit and sustain the growth of heterotrophic, soil-borne bacteria. This process resembles the  
311 establishment of the microbial communities that associate with the roots and rhizospheres of land  
312 plants, suggesting common organizational principles shared between chlorophytes and  
313 embryophytes. Our in-depth characterization of the *Cr* microbiota shows clear differences as well  
314 as striking similarities in the taxonomic affiliation of abundant root and phycosphere community  
315 members (Fig. 1D). Notably, these similarities are found despite biochemical differences between  
316 extracellular organic carbon compounds released by *At* roots and *Cr*, as well as by differences in  
317 cell wall composition, which in the case of the plant root mostly consists of complex  
318 polysaccharides such as cellulose, whereas in *Cr* it is primarily composed of (glyco)proteins  
319 (Harris, 2009). Among the bacterial lineages shared between the root and phycosphere  
320 microbiota, we found groups that are known to establish intimate interactions with multicellular  
321 plants, ranging from symbiotic to pathogenic, such as Rhizobia, *Pseudomonas*, *Burkholderia*, or  
322 *Xanthomonas* (Suarez-Moreno, 2014; Garrido-Oter *et al.*, 2018; Karasov *et al.*, 2018; Timilsina *et*  
323 *al.*, 2020). Meta-analyses of available data from multiple studies further confirm this pattern by  
324 revealing the presence of a set of six bacterial orders, found as abundant members not only in the  
325 root communities of all analyzed land plants, but also in the *Cr* phycosphere (Fig. 2). These  
326 findings suggest that the capacity to associate with a wide range of photosynthetic organisms is a  
327 common trait of these core bacterial taxa, which might predate the emergence of more specialized  
328 forms of interaction with their host. This hypothesis was implicitly tested in our cross-inoculation  
329 gnotobiotic experiments, where bacterial strains originally isolated from the roots of *At* or the

330 phycosphere of *Cr* competed for colonization of either host (**Fig. S1E**). The observation that *Cr*-  
331 derived strains could colonize *At* roots in a competition setup, whereas *At*-derived bacterial  
332 SynComs also populated *Cr* phycospheres (**Fig. 5C**) supports the existence of shared bacterial  
333 traits for establishing general associations with photosynthetic hosts. Despite these patterns of  
334 ectopic colonization, we also detected significant signatures of host preference, illustrated by the  
335 observation that native bacterial SynComs outcompeted non-native strains in the presence of  
336 either host, but not in their absence (**Fig. 5C**). These findings are in line with a recent comparative  
337 microbiota study where similar results were observed for bacterial commensals from two species  
338 of land plants (*A. thaliana* and *L. japonicus*; [Wippel et al., 2021](#)). In addition, SynComs composed  
339 of strains exclusively derived from the *At*- or the *Cr*-SPHERE collections, assembled into  
340 taxonomically equivalent communities on either host, which were indistinguishable at the family  
341 level (**Fig. 5A-B**). Together, our findings suggest that these bacterial taxa have in common the  
342 ability to assemble into robust communities and associate with a wide range of photosynthetic  
343 organisms, including unicellular algae and flowering plants.

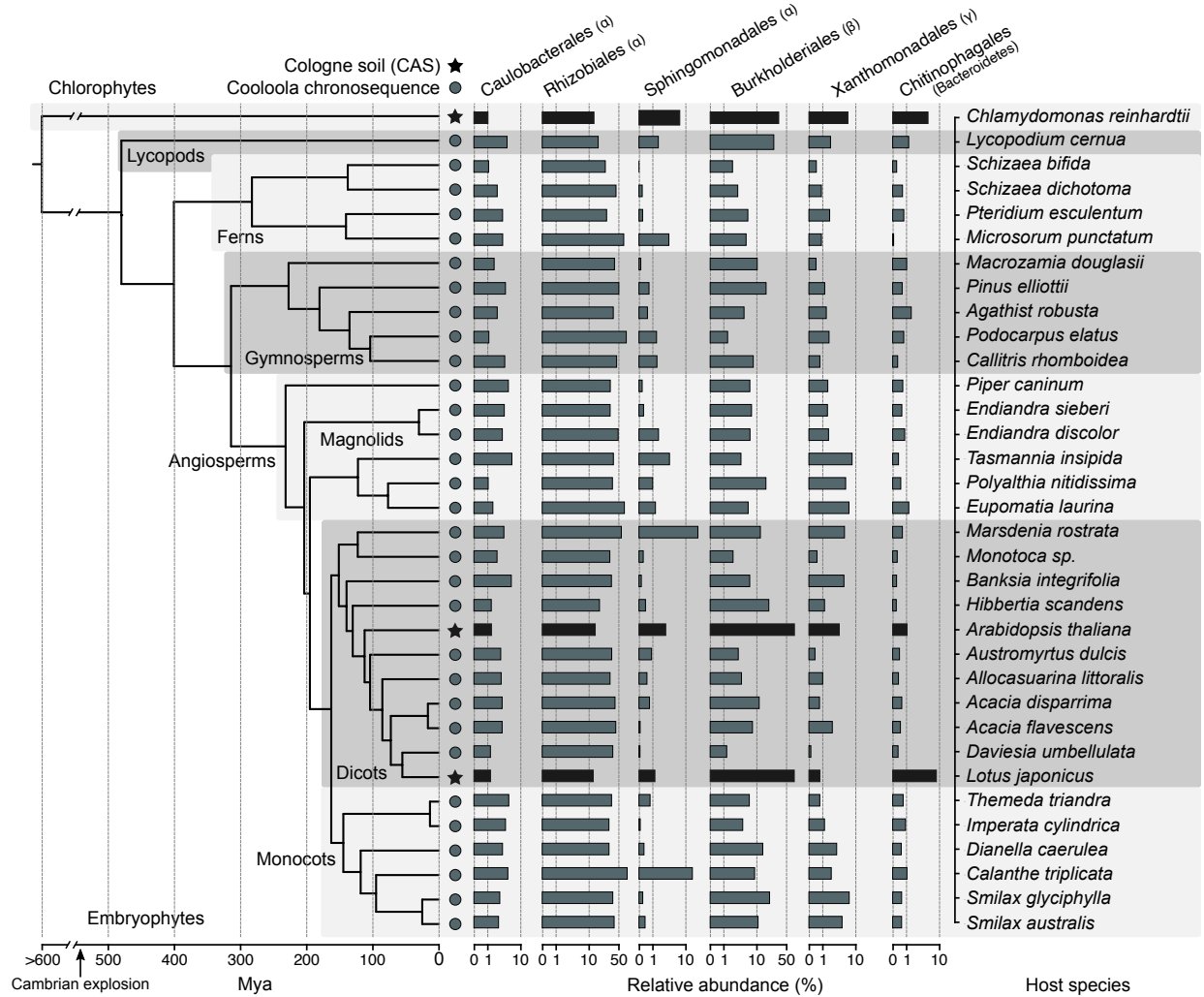
344 Carbon is assumed to be the main factor limiting bacterial growth in soil ([Demoling et al., 2007](#)).  
345 Thus, secretion of organic carbon compounds by photosynthetic organisms constitutes a strong  
346 cue for the assembly of soil-derived microbial communities ([Bulgarelli et al., 2013](#); [Zhalnina et al.,](#)  
347 [2018](#); [Huang et al., 2019](#)). The observed similarities between the root and phycosphere microbiota  
348 at a high taxonomic level suggest that the release of photoassimilates acts as a first organizing  
349 principle driving the formation of these communities. This hypothesis is also supported by a recent  
350 study with marine bacterial mesocosms where community composition could be partially predicted  
351 by the addition of phytoplankton metabolites ([Fu et al., 2020](#)). However, the results from our split  
352 system (**Fig. S1F** and **Fig. 6**), where bacterial SynComs formed distinct communities and had a  
353 beneficial effect on *Cr* growth depending on their physical proximity, indicate that the provision of  
354 diffusible carbon compounds is not sufficient to explain the observed patterns of microbial  
355 diversity. In addition, shed *Cr* cell wall components, which may not be diffusible through the 0.22  
356  $\mu\text{m}$ -pore membrane, could be degraded by bacteria only in close proximity. The importance of  
357 proximity to the algal cells could also be a consequence of gradients in concentrations and  
358 variations in the diffusivity of different compounds, which in aquatic environments is predicted to  
359 cause highly chemotactic, copiotrophic bacterial populations to outcompete low-motility  
360 oligotrophic ones ([Smriga et al., 2016](#)). Together with the algal growth data, the observed  
361 variations in SynCom structures suggest that, in addition to physical proximity, bi-directional  
362 exchange of metabolic currencies and / or molecular signals may be required for the assembly  
363 and sustained growth of a phycosphere microbiota capable of providing beneficial functions to

364 their host. Future experimentation using this system will be aimed at elucidating core molecular  
365 and ecological principles that govern interactions between photosynthetic organisms and their  
366 microbiota.



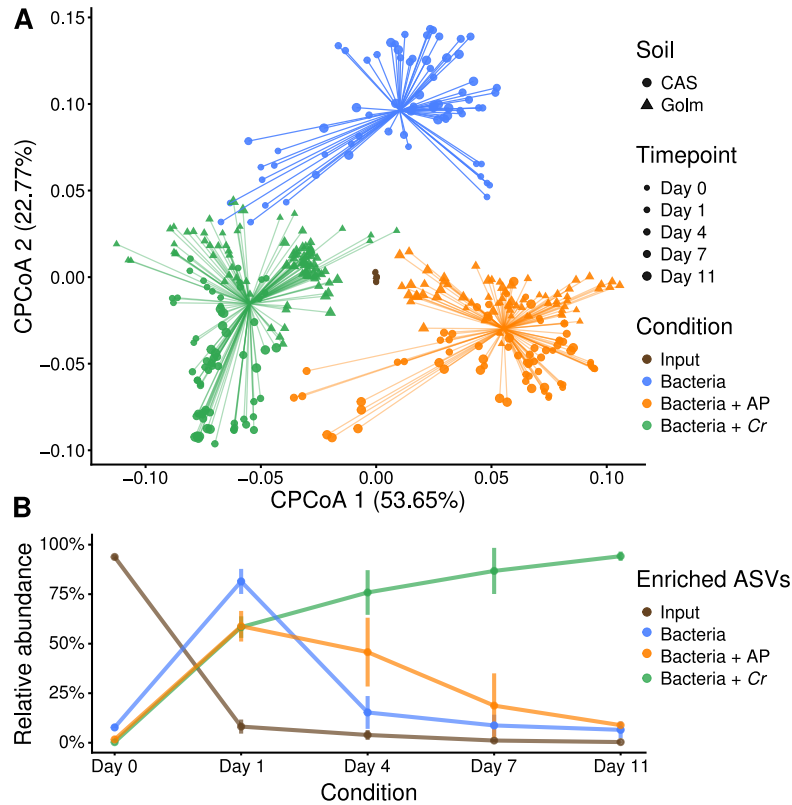
367

368 **Figure 1. Comparison of bacterial community structures associated with *At* roots and the**  
 369 ***Cr* phycosphere in natural soil. (A)** Alpha diversity estimates of soil, rhizosphere, root and  
 370 phycosphere samples from *At* and *Cr* grown in CAS soil in the greenhouse. **(B-C)** PCoA of Bray-  
 371 Curtis dissimilarities constrained by compartment (22.4% of variance explained;  $P < 0.001$ ). A  
 372 separation between root, phycosphere and soil-derived samples can be observed in the first two  
 373 components **(B)**, while the root and phycosphere communities cluster together in the second and  
 374 third PCoA axes **(C)**. **(D)** Phylogeny of 16S rRNA sequences of the most abundant OTUs found  
 375 in *At* roots and *Cr* phycosphere community profiles. Leaf nodes are colored by taxonomic affiliation  
 376 (phylum level). The two innermost rings (colored squares) represent abundant OTUs in each  
 377 compartment. Squares highlighted with a black contour correspond to OTUs for which at least one  
 378 representative bacterial strain exists in the IRL or IPL culture collections. The two outermost rings  
 379 (barplots) represent log-transformed relative abundances of each OTU in *At* root or *Cr*  
 380 phycosphere samples.



381  
382 **Figure 2. Conservation of bacterial orders of the root and phycosphere microbiota across**  
383 **photosynthetic organisms.** Phylogeny inferred from a multiple sequence alignment of the  
384 ribulose-bisphosphate carboxylase gene (*rbcl*) of 35 plant species and *Chlamydomonas*  
385 *reinhardtii*. The barplots represent the average aggregated relative abundance of the six bacterial  
386 orders found to be present in the root microbiota of each plant species (80% occupancy and  $\geq 0.1\%$   
387 average relative abundance). Leaf nodes depicted with a star symbol denote community profiles  
388 of plants grown in CAS soil in the greenhouse (Thiergart *et al.*, 2019; Harbort *et al.*, 2020), whereas  
389 those marked with a circle were obtained from plants sampled at the Cooloola natural site  
390 chronosequence (Yeoh *et al.*, 2017).

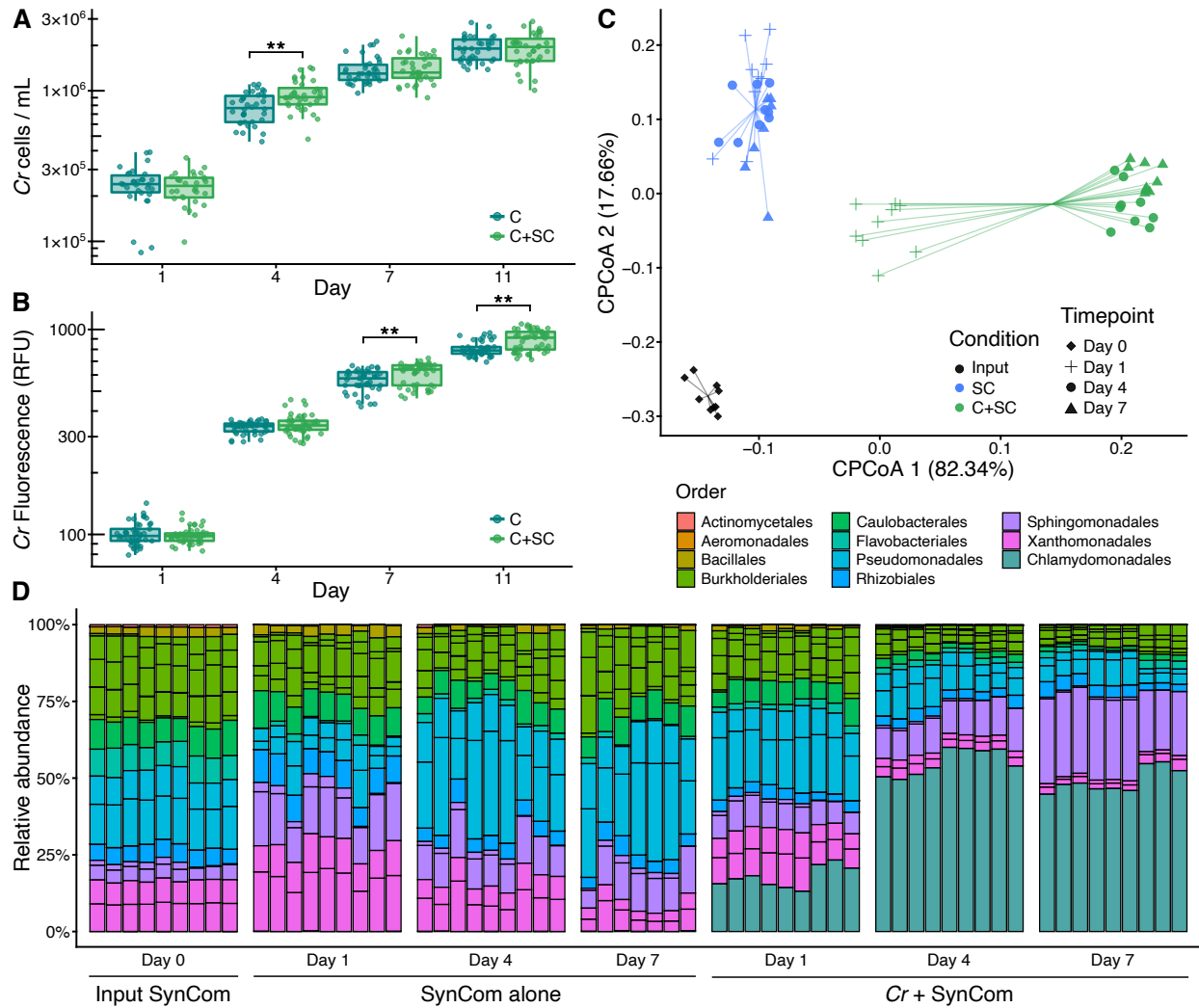




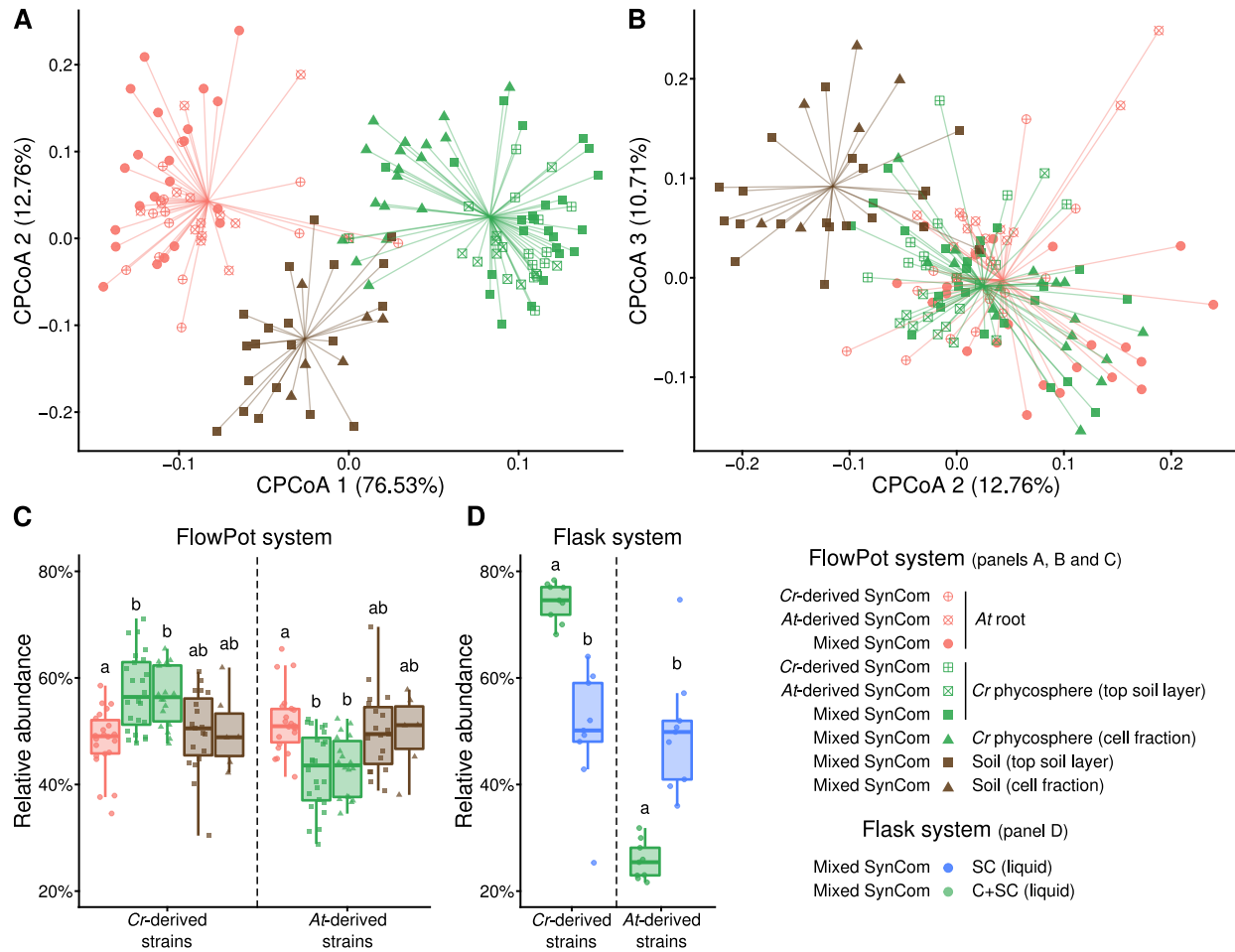
391

392 **Figure 3. Mesocosm experiments recapitulate the establishment of phycosphere**  
393 **communities by *Cr* across soil types and growth media.**

394 **(A)** PCoA analysis of Bray-Curtis dissimilarities constrained by condition (17.9% of variance;  
395  $P < 0.001$ ) show a significant separation between start inocula (soil washes, depicted in brown),  
396 phycosphere communities (green), and soil washes incubated in minimal media (blue), or media  
397 supplemented with artificial photoassimilates (APs, depicted in orange). **(B)** Dynamic changes in  
398 the phycosphere community composition in terms of the aggregate relative abundances of ASVs  
399 enriched in each condition with respect to the start inocula.

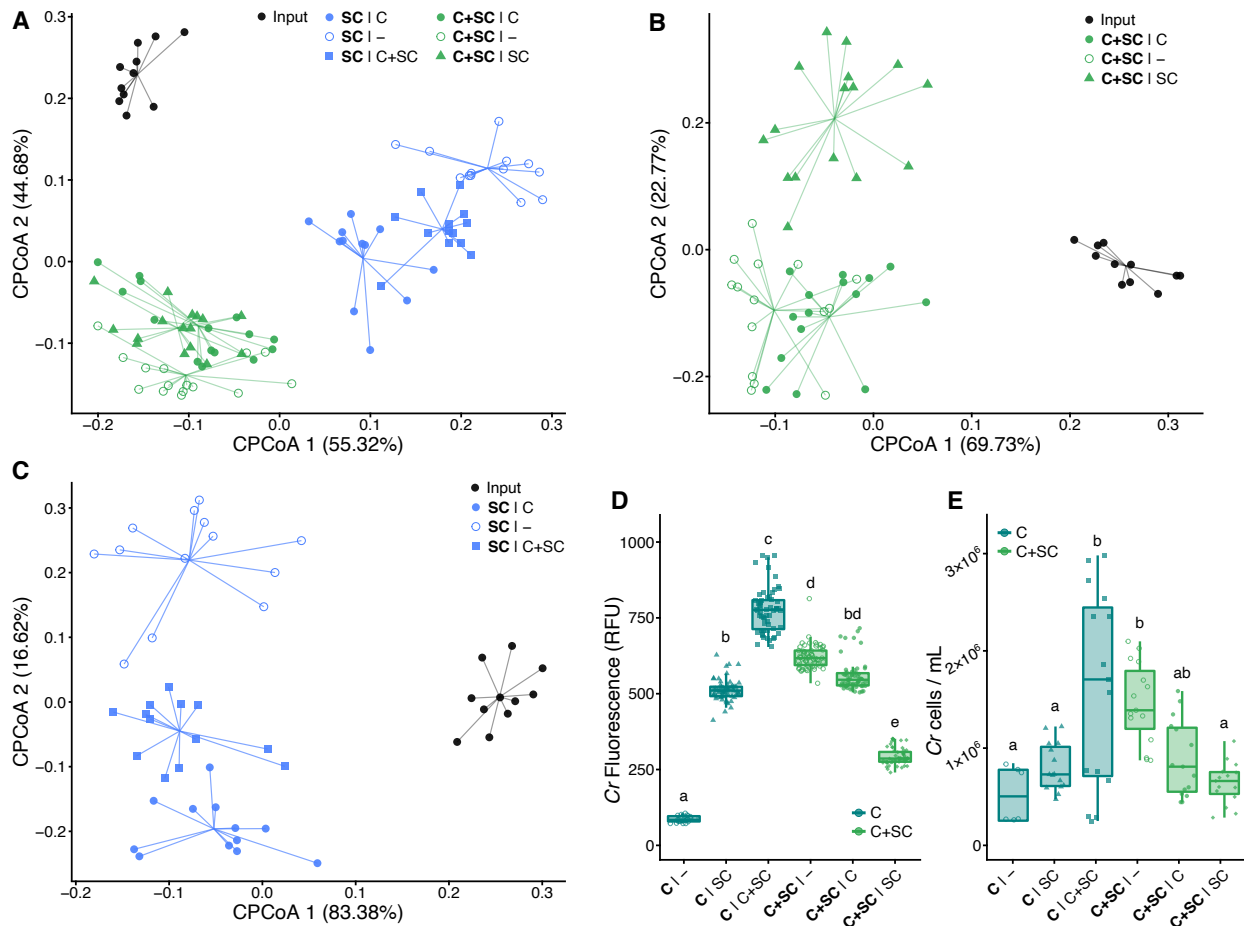


400  
 401 **Figure 4. Phycosphere reconstitution using bacterial SynComs derived from the *Cr*-**  
 402 **SPHERE core culture collection. (A)** Beta-diversity analysis (CPCoA of Bray-Curtis  
 403 dissimilarities; 40.4% of the variance;  $P < 0.001$ ) of samples obtained from a liquid-based  
 404 gnotobiotic system, showing a significant separation between input SynCom samples (black),  
 405 synthetic phycospheres (light green), and SynCom only controls (blue). **(B)** Bar charts showing  
 406 relative abundances of individual SynCom members across conditions and timepoints (colored by  
 407 their taxonomic affiliation at the order level). **(C-D)** *Chlamydomonas* growth in the gnotobiotic  
 408 system axenically (dark green) or in co-inoculation with the bacterial SynCom (light green),  
 409 measured as algal cell densities **(C)**, and relative chlorophyll fluorescence **(D)**.



410

411 **Figure 5. Root and phycosphere bacteria colonize *At* and *Cr* and assemble into**  
 412 **taxonomically equivalent communities. (A-B)** Beta diversity analysis of soil, root, and  
 413 phycosphere community profiles obtained from gnotobiotic *At* and *Cr*, inoculated with bacterial  
 414 SynComs derived from *At* roots (*At*-SPHERE), *Cr* (*Cr*-SPHERE) or mixed (*At*- and *Cr*-SPHERE),  
 415 grown in the FlowPot system analysis (CPCoA of Bray-Curtis dissimilarities aggregated at the  
 416 family level; 16.4% of the variance;  $P < 0.001$ ). Similar as in natural soils (**Fig. 1B-C**), root and  
 417 phycosphere samples were significantly separated from soil and from each other in the first two  
 418 axes, while overlapping in the second and third components. (**C-D**) Aggregated relative  
 419 abundances of *At*- and *Cr*-derived strains in the mixed SynCom show ectopic colonization and  
 420 signatures of host preference in a soil-derived (FlowPot, panel **C**), and liquid-based (flask, panel  
 421 **D**) gnotobiotic system.



422

423 **Figure 6. Physical proximity to *Cr* is required for the establishment of phycosphere**  
 424 **bacterial communities.** Beta-diversity analyses of Bray-Curtis dissimilarities of SynComs grown  
 425 in a split gnotobiotic system show a significant separation of samples according physical proximity  
 426 to *Cr* (21% of variance;  $P < 0.001$ , **A**), or the content of the neighboring vessel (39.4-39.5% of  
 427 variance;  $P < 0.001$ , panels **B-C**). (**D-E**) *Cr* growth across conditions measured using relative  
 428 chlorophyll fluorescence (RFU; panel **D**) and algal cell densities (panel **E**).

## 429 **Methods**

### 430 ***Cr* culture conditions**

431 *Cr* CC1690 cells were grown photoautotrophically in TP (Kropat *et al.*, 2011), TP10 or B&D  
432 medium (Broughton and Dilworth, 1971) at 25 °C, and an illumination of 125  $\mu\text{mol m}^{-2} \text{s}^{-1}$  under  
433 continuous light conditions. Cultures were kept in a rotatory shaker at 70 RPM. Cells in the mid-  
434 logarithmic phase were used as inocula for the different experiments. Cell growth was determined  
435 either by measuring samples in a Multisizer 4e Coulter counter (Beckman Coulter Inc., California,  
436 USA) or using an Infinite M200Pro (TECAN Austria GmbH, Grödig, Austria) plate reader to  
437 determine either absorbance at 750 nm or chlorophyll fluorescence (excitation 440/9 nm, emission  
438 680/20 nm).

### 439 **Greenhouse experiment**

440 *Arabidopsis thaliana* Col-0 seeds were surface-sterilized in 70% ethanol for 10 min followed by a  
441 brief wash with 100% ethanol (1 min), a wash with 3% NaClO (1 min) and five subsequent washes  
442 with sterile water. Seeds imbibed in sterile water were stratified for four days at 4°C in the dark.  
443 Five seeds were then directly sown onto the surface of pots containing Cologne Agricultural Soil  
444 (CAS) by pipetting one seed at a time.

445 After 36 days plants were harvested similarly to previously reported protocols (Thiergart *et al.*,  
446 2020). Briefly, and plant roots were manually separated from the surrounding soil, until only tightly  
447 adhered soil particles were left. Then, roots were separated from their shoot and placed in a Falcon  
448 tube with 10 mL of deionized sterile water. After ten inversions, the roots were transferred to  
449 another Falcon tube and further processed, while leftover wash-off was centrifuged at 4,000 $\times$ g for  
450 10 min. The supernatant was discarded and the pellet was resuspended and transferred to a new  
451 2-mL screw-cap tube. This tube was centrifuged at 20,000 RPM for 10 min, the supernatant was  
452 discarded and the pellet snap-frozen in liquid nitrogen and stored for further processing  
453 (rhizosphere compartment). Root systems were then washed successively in 80% EtOH and 3%  
454 NaOCl to further clean the root surfaces from living microorganisms and subsequently washed  
455 three times (1 min each) in sterile water. These microbe-enriched root fractions were transferred  
456 to 2-mL screw-cap tubes for further processing (**Fig S1A**).

457 Liquid TP cultures of 7-day old *Cr* (CC1690) were washed by sequential centrifugation at 5,000 $\times$ g  
458 for 5 min and resuspended in 50 mL of  $\text{MgCl}_2$ , to an average  $1.4 \times 10^6$  cells/mL across biological  
459 replicates, to be used as inocula for CAS pots. Samples from the surface of the *Cr*-inoculated pots  
460 were collected using an ethanol-washed metal spatula at 7, 14, 21, 28, and 36 days post-

461 inoculation. Unplanted pots containing CAS were used to collect surface samples as mock-  
462 treatment control right after inoculation (day 0) and at the same time points as *Cr*-inoculated pots.  
463 The position of the pots in the trays was shuffled periodically to minimize edge and location effects  
464 (**Fig S1A**). Sterile petri dishes were placed at the bottom of each pot, which were then watered  
465 from the top at inoculation time with 50 mL of MgCl<sub>2</sub>, and then by adding sterile MilliQ water every  
466 2-3 days in the petri dishes, and kept in the greenhouse under long-day conditions (16/8 h  
467 light/dark). Collected samples were snap-frozen using liquid nitrogen and stored at -80 °C until  
468 further processing.

#### 469 **Microbial soil wash preparation**

470 Soil samples (5 g) from CAS or GOLM soil were collected in Falcon tubes and manually  
471 resuspended onto 30 mL of sterile 1x Tris-EDTA (TE) supplemented with 0.1% of Triton X-100  
472 (SERVA Electrophoresis GmbH, Heidelberg, Germany). The solution was then homogenized by  
473 inversion at 40 RPM for 30 min in a rotary mixer and centrifuged for 1 min at 1500 RPM to remove  
474 bigger soil particles. Afterwards, the supernatant was transferred to a new Falcon tube and  
475 centrifuged at 4,000×g for 20 min. After centrifugation the supernatant was discarded and the  
476 pellet resuspended in 50 mL of the final medium. Cell concentration was then determined using  
477 either a hemocytometer or the Multisizer 4e.

478 *Cr* cells from an axenic culture were inoculated to a density of 10<sup>5</sup> cells/mL into 50 mL of TP or  
479 B&D medium in triplicate in 200mL flasks. An estimate of 10<sup>9</sup> cells from the microbial soil wash  
480 were added to the same flasks and incubated for 11 days as described above. Controls consisted  
481 in flasks, wrapped in aluminum foil to prevent the pass of light, containing the same growth media  
482 as the one used for the *Cr* cultures with and without artificial photosynthates (AP; [Baudoin et al.,](#)  
483 [2003](#)). Samples were collected for DNA extraction and cell counts determination at 0, 1, 4, 7, and  
484 11 days post inoculation (**Fig S1B**). These experiments were repeated in three biologically  
485 independent experiments, per soil type and growth media.

#### 486 **DNA extraction from soil samples**

487 Total DNA was extracted from the aforementioned samples using the FastDNA™ SPIN Kit for Soil  
488 following instructions from the manufacturer (MP Biomedicals, Solon, USA). DNA samples were  
489 eluted in 50 µL nuclease-free water and used for microbial community profiling.

#### 490 **DNA extraction from liquid samples**

491 DNA from liquid samples was extracted using alkaline lysis ([Bai et al., 2015](#)). Briefly, 12 µL of the  
492 sample were diluted in 20 µL of Buffer I (NaOH 25 mM, EDTA(Na) 0.2mM, pH 12), mixed by



493 pipetting and incubated at 94 °C for 30 min. Next, 20 µL of Buffer II (Tris-HCl 40 mM, pH 7.46)  
494 were added to the mixture and stored at -20 °C.

#### 495 **Isolation and genome sequencing of *Chlamydomonas*-associated bacteria**

496 Soil bacteria associated with *Cr* after co-cultivation were isolated from mesocosm cultures using  
497 a dilution-to-extinction approach (Bai *et al.*, 2015; Wippel *et al.*, 2021). Briefly, cultures containing  
498 *Cr* and bacteria from CAS soil washes as described above were incubated in TP or B&D media.  
499 After 7 days of co-cultivation mesocosm samples were fractionated by sequential centrifugation  
500 and sonication (Fig. S1C; Kim *et al.*, 2014) prior to dilution. For fractionation, cultures were  
501 centrifuged at 400×g for 5 min to recover the supernatant. The pellet was washed with 1x TE  
502 buffer followed by sonication in a water bath at room temperature for 10 min and centrifugation at  
503 1,000×g for 5 min. The supernatant from the first and second centrifugation were pooled together  
504 and diluted at either 1:10,000 or 1:50,000. Diluted supernatants were then distributed into 96-well  
505 microtiter plates containing 20% TSB media. After 3 weeks of incubation in the dark at room  
506 temperature, plates that showed visible bacterial growth were chosen for 16S rRNA amplicon  
507 sequencing. For identification of the bacterial isolates, a two-step barcoded PCR protocol was  
508 used as previously described (Wippel *et al.*, 2021). Briefly, DNA extracted from the isolates was  
509 used to amplify the v5-v7 fragments of the 16S rRNA gene by PCR using the primers 799F  
510 (AACMGGATTAGATACCCKG) and 1192R (ACGTCATCCCCACCTTCC), followed by indexing  
511 of the PCR products using Illumina-barcoded primers. The indexed 16S rRNA amplicons were  
512 subsequently pooled, purified, and sequenced on the Illumina MiSeq platform. Next, cross-  
513 referencing of IPL sequences with mesocosm profiles allowed us to identify candidate strains for  
514 further characterization, purification, and whole-genome sequencing. Two main criteria were used  
515 for this selection: first, we aimed at obtaining maximum taxonomic coverage and selected  
516 candidates from as many taxa as possible; second, we gave priority to strains whose 16S  
517 sequences were highly abundant in the natural communities. Whenever multiple candidates from  
518 the same phylogroup were identified, we aimed at obtaining multiple independent strains, if  
519 possible, coming from separate biological replicates to ensure they represented independent  
520 isolation events. After validation of selected strains, 185 were successfully subjected to whole-  
521 genome sequencing. Liquid cultures or swabs from agar plates from selected bacterial strains  
522 (Supplementary Data 3) were used to extract DNA using the QiAmp Micro DNA kit (Qiagen,  
523 Hilden, Germany). The extracted DNA was treated with RNase, and purified. Quality control,  
524 library preparation, and sequencing (2 x 150 bp; Illumina HiSeq3000) at a 4-5 million reads per  
525 sample were performed by the Max Planck-Genome Center, Cologne, Germany  
526 (<https://mpgc.mpiiz.mpg.de/home/>).

## 527 **Multi-species microbiota reconstitution experiments**

528 The gnotobiotic FlowPot (Kremer *et al.*, 2021) system was used to grow *Cr* or *A. thaliana* plants  
529 with and without bacterial SynComs. This system allows for even inoculation of each FlowPot with  
530 microbes by flushing of the pots with the help of a syringe attached to the bottom opening. After  
531 FlowPot assemblage, sterilization and microbial inoculation sterilized seeds were placed on the  
532 matrix (peat and vermiculite, 2:1 ratio), and pots were incubated under short-day conditions (10  
533 hours light, 21°C; 14 hours dark, 19°C), standing in customized plastic racks in sterile  
534 'TP1600+TPD1200' plastic boxes with filter lids (SacO2, Deinze, Belgium). For SynCom  
535 preparation, bacterial strains from either *Cr*- or *At*-SPHERE were grown separately in liquid culture  
536 for 2-5 days in 50% TSB media and then centrifuged at 4,000 xg for 10 min and re-suspended in  
537 10 mM MgCl<sub>2</sub> to remove residual media and bacteria-derived metabolites. Equivalent ratios of  
538 each strain, determined by optical density (OD<sub>600</sub>) were combined to yield the desired SynComs  
539 (**Table S1**). An aliquot of the SynComs as reference samples for the experiment microbial inputs  
540 were stored at -80°C for further processing. SynCom bacterial cells (10<sup>7</sup>) were added to either 50  
541 mL of TP10 or ½ MS (Duchefa Biochemie, Haarlem, Netherlands), which were then inoculated  
542 into the FlowPots using a 60 mL syringe. For *Cr*-inoculated pots, 10<sup>5</sup> of washed *Cr* cells were  
543 added to the 50mL of media with or without microbes to be inoculated into the FlowPots.

544 *Chlamydomonas* or *Arabidopsis* FlowPots were grown side-by-side in gnotobiotic boxes, with six  
545 pots in total per box. This experiment was repeated in three independent biological replicates.  
546 After five weeks of growth, roots were harvested and cleaned thoroughly from attached soil using  
547 sterile water and forceps. Surface of *Chlamydomonas* pots were used as phycosphere samples  
548 (cells were harvested from visibly green surface areas, top soil samples). In addition, to remove  
549 any possible background effect from carry-over soil particles, the surface-harvested samples were  
550 washed in sterile TE supplemented with 0.1% of Triton X-100 by manually shaking in 2-mL  
551 Eppendorf tubes. Then, the tubes rested for a few minutes and the supernatant was used as "cell  
552 fraction" samples. Finally, soil from unplanted pots were collected as soil samples and treated  
553 similarly as *Chlamydomonas*-inoculated pots for microbial community comparison. All  
554 phycosphere, root (comprising both the epiphytic, and endophytic compartments), and soil (soil  
555 from unplanted pots) samples were transferred to Lysing Matrix E tubes (MP Biomedicals, Solon,  
556 USA), frozen in liquid nitrogen, and stored at -80°C for further processing. DNA was isolated from  
557 those samples using the MP Biomedicals FastDNA™ Spin Kit for Soil, and from the input SynCom  
558 by alkaline lysis, and subjected to bacterial community profiling.

559 To ensure sufficient surface for phycosphere harvesting, we set up an additional experiment based  
560 on sterile peat without FlowPots. Experiments with the mixed SynCom of *Cr*- and *At*-SPHERE

561 strains were conducted using sterile 'TP750+TPD750' plastic boxes (SacO2, Deinze, Belgium).  
562 Sterile soil and vermiculite were mixed in a 2:1 ratio and added to each box. Next, the boxes were  
563 inoculated by adding 95 mL of TP10 or ½ MS, for the *Chlamydomonas* or *Arabidopsis* boxes  
564 respectively, containing  $2 \times 10^7$  bacterial cells.

565 Samples for chlorophyll extraction were collected from the different *Chlamydomonas* containing  
566 gnotobiotic systems by harvesting the green surface of the peat and extracting the cells as  
567 described above. Then, 1 mL of these extracts were centrifuged at 14,000 xg for 1 min at 4°C with  
568 2.5 µl 2% (v/v) Tween 20 (Sigma-Aldrich, Darmstadt, Germany) to promote the aggregation into  
569 a pellet. Then, the supernatant was completely removed and the pellets stored at -80°C until  
570 extraction.

### 571 **Chlorophyll extraction from algae-containing samples**

572 From each extracted cell samples from the gnotobiotic soil system, 1 mL was collected and mixed  
573 with 2.5 µL of 2% (v/v) Tween 20 in 1.5 mL Eppendorf tubes. The samples were centrifuged for 1  
574 min at 14,000×g and 4 °C, then the supernatant was removed and the pellet stored at -80 °C.  
575 Frozen samples were thawed on ice for 2 min and 1 mL of HPLC grade methanol (Sigma, 34860-  
576 4L-R) added to the pellets. The tubes were covered from the light using aluminum foil and mixed  
577 using the vortex for 1 min. After vortexing, the cells were incubated in the dark at 4 °C for five  
578 minutes. Next, the pigments were obtained by centrifuging the cells for 5 minutes at maximum  
579 speed and 4 °C and recovering the supernatant. The pigments absorbance at 652 and 665 nm  
580 was measured in a plate reader Infinite M200Pro using methanol as blank. The absorbance values  
581 were then substituted in the following equation  $\text{Chl a} + \text{Chl b} = 22.12 \times \text{Abs}_{652} + 2.71 \times \text{Abs}_{665}$  (Porra  
582 *et al.*, 1989).

### 583 **Split co-cultivation system**

584 Co-cultivation devices were built by adapting 150 mL Stericup-GV filtration devices (Merck  
585 Millipore, Darmstadt, Germany) harboring a 0.22 µm filter membrane (Alvarez and Cava, 2018).  
586 Each co-cultivation device was assembled inside a clean hood 150 mL and 100 mL of TP10 were  
587 added into the big and small chamber of the filtration device, respectively. Chambers were  
588 inoculated at different cell concentrations depending on the content of the chamber (Fig S1F).  
589 The concentrations used were  $10^5$  and  $10^7$  cells/mL for *Chlamydomonas* and SynCom  
590 respectively. For the C+SC condition, the inoculum concentration was the same as for individual  
591 content chambers. After inoculation the devices were transferred to a shaking platform and  
592 incubated under the same conditions used for *Cr* liquid cultures described above. Four samples  
593 per chamber were harvested for DNA extraction, fluorescence, and cell growth at the start of the

594 incubation and 7 days after inoculation. These experiments were repeated in three independent  
595 biological replicates, containing one technical replicate each.

596 Additionally, a full-factorial replicate of the experiment was carried out using a custom-made co-  
597 cultivation device (Cat. #0250 045 25, WLB Laborbedarf, Möckmühl, Germany). Briefly, two 250  
598 mL borosilicate glass bottles (**Fig. S1F**) were modified by adding on the sidewall of each bottle a  
599 glass neck with a NW25 flange. The flange holds a disposable 0.22  $\mu\text{m}$ -pore PVDF Durapore  
600 filtration membrane (Merck Millipore, Darmstadt, Germany) and is kept in place by an adjustable  
601 metal clamp. In this device, each bottle holds 150 mL of TP10 and the initial cell concentrations  
602 were the same as the ones used in the previously described co-cultivation device. Similar to the  
603 Stericup system, four samples per chamber were harvested for DNA extraction. Chlorophyll  
604 fluorescence and cell growth measurements were collected at the start of the incubation and 7  
605 days after inoculation. These experiments were repeated in three independent biological  
606 replicates, containing one technical replicate each.

#### 607 **Preparation of SynCom inocula**

608 Bacterial cultures from the strains selected for the different SynComs (**Supplementary Data 4**)  
609 were started from glycerol stocks which were used to streak agar plates containing TSA 50%  
610 media. Plates were cultured at 25 °C for five days and later used to inoculate culture tubes with 1  
611 mL of 50% TSB media. The tubes were incubated for six days at 25 °C and 180 RPM. After 6  
612 days, the cultures were washed three times by centrifugation at 4,000  $\times g$  for 5 min, the supernatant  
613 discarded, and the pellet resuspended into 2 mL of TP or TP10 media. The washed cultures were  
614 further incubated with shaking at 25 °C for an additional day. Bacterial concentration in washed  
615 cultures was determined by measuring OD<sub>600</sub> and, subsequently pooled in equal ratios. Cell counts  
616 of the pooled SynCom were measured using the Multisizer 4e and adjusted to 10<sup>6</sup>, to inoculate  
617 together with 10<sup>4</sup> cells of *Cr* (prepared as described above) in 50 mL of TP10 in 200-mL flasks.  
618 These flasks were inoculated in triplicate and three biological replicates were prepared for both  
619 bacteria and *Cr* start inocula. As controls, *Cr*-only cultures and SynCom-only cultures were  
620 incubated in parallel, and samples taken at 0, 1, 4, 7 for community profiling, and at 0, 4, 7, 14  
621 days for *Cr* cell counts.

#### 622 **Culture-independent bacterial 16S rRNA sequencing**

623 DNA samples were used in a two-step PCR amplification protocol. In the first step, V2–V4 (341F:  
624 CCTACGGGNGGCWGCAG; 806R: GGACTACHVGGGTWTCTAAT) or V4-V7 (799F:  
625 AACMGATTAGATACCCKG; 1192R: ACGTCATCCCCACCTTCC) of bacterial 16S rRNA were  
626 amplified. Under a sterile hood, each sample was amplified in triplicate in a 25  $\mu\text{L}$  reaction volume

627 containing 2 U DFS-Taq DNA polymerase, 1x incomplete buffer (Bioron GmbH, Ludwigshafen,  
628 Germany), 2 mM MgCl<sub>2</sub>, 0.3% BSA, 0.2 mM dNTPs (Life technologies GmbH, Darmstadt,  
629 Germany) and 0.3 μM forward and reverse primers. PCR was performed using the same  
630 parameters for all primer pairs (94°C/2 min, 94°C/30 s, 55°C/30 s, 72°C/30 s, 72°C/10 min for 25  
631 cycles). Afterwards, single-stranded DNA and proteins were digested by adding 1 μL of Antarctic  
632 phosphatase, 1 μL Exonuclease I and 2.44 μL Antarctic Phosphatase buffer (New England  
633 BioLabs GmbH, Frankfurt, Germany) to 20 μL of the pooled PCR product. Samples were incubated  
634 at 37°C for 30 min and enzymes were deactivated at 85°C for 15 min. Samples were centrifuged  
635 for 10 min at 4,000 rpm and 3 μL of this reaction were used for a second PCR, prepared in the  
636 same way as described above using the same protocol but with cycles reduced to 10 and with  
637 primers including barcodes and Illumina adaptors. PCR quality was controlled by loading 5 μL of  
638 each reaction on a 1% agarose gel and affirming that no band was detected within the negative  
639 control. Afterwards, the replicated reactions were combined and purified. In the case of bacterial  
640 amplicons with possible plant DNA PCR products, amplicons were loaded on a 1.5% agarose gel  
641 and run for 2 hours at 80 V. Subsequently, bands with a size of ~500 bp were cut out and purified  
642 using the QIAquick gel extraction kit (Qiagen, Hilden, Germany). If plant DNA PCR products were  
643 not present, bacterial amplicons were purified with Agencourt AMPure XP beads DNA  
644 concentration was fluorescently determined, and 30 ng DNA of each of the barcoded amplicons  
645 were pooled in one library. The library was then purified and re-concentrated twice with Agencourt  
646 AMPure XP beads, and pooled in similar ratios for sequencing. Paired-end Illumina sequencing  
647 was performed in-house using the MiSeq sequencer and custom sequencing primers  
648 (**Supplementary Data 5**).

#### 649 **Analysis of culture-independent bacterial 16S rRNA profiling**

650 Amplicon sequencing data from *Cr* or *At* roots grown in CAS soil in the greenhouse, along with  
651 unplanted controls, were demultiplexed according to their barcode sequence using the QIIME  
652 pipeline (Caporaso *et al.*, 2010). Afterwards, DADA2 (Callahan *et al.*, 2016) was used to process  
653 the raw sequencing reads of each sample. Unique amplicon sequencing variants (ASVs) were  
654 inferred from error-corrected reads, followed by chimera filtering, also using the DADA2 pipeline.  
655 Next, ASVs were aligned to the SILVA database (Quast *et al.*, 2013) for taxonomic assignment  
656 using the naïve Bayesian classifier implemented by DADA2. Raw reads were mapped to the  
657 inferred ASVs to generate an abundance table, which was subsequently employed for analyses  
658 of diversity and differential abundance using the R package *vegan* (Oksanen *et al.*, 2019).

659 Amplicon sequencing reads from the *Cr* IPL and from the corresponding mesocosm culture-  
660 independent community profiling were quality-filtered and demultiplexed according to their two-



661 barcode (well and plate) identifiers using custom scripts and a combination of tools included in the  
662 QIIME and USEARCH (Edgar *et al.*, 2010) pipelines. Next, sequences were clustered into  
663 Operational Taxonomic Units (OTUs) with a 97% sequence identity similarity using the UPARSE  
664 algorithm, followed by identification of chimeras using UCHIME (Edgar *et al.*, 2011). Samples from  
665 wells with fewer than 100 good quality reads were removed from the data set as well as OTUs not  
666 found in a well with at least ten reads. Recovery rates (Figure S4A). were estimated by calculating  
667 the percentage of the top 100 most abundant OTUs found in natural communities (greenhouse  
668 experiment) that had at least one isolate in the culture collection (62%), and the total aggregated  
669 relative abundances of recovered OTUs (63%). We identified IPL samples matching OTUs found  
670 in the culture-independent root samples and selected a set of 185 representative strains  
671 maximizing taxonomic coverage for subsequent validation and whole-genome sequencing,  
672 forming the basis of the *Cr*-SPHERE collection.

### 673 **Meta-analysis of phycosphere and root microbiota profiles**

674 For the meta-analysis of root microbiota samples across plant species, data from previous studies  
675 of *Arabidopsis* and *Lotus* grown in CAS soil (Thiergart *et al.*, 2019; Harbort *et al.*, 2020) were  
676 processed using the pipeline described above and merged with samples obtained from the  
677 Cooloola natural site chronosequence (Yeoh *et al.*, 2017). Sequencing reads from this latter study  
678 (Roche 454) were quality filtered and trimmed after removal of primer sequences. Given that these  
679 studies employed non-overlapping sequencing primers, all datasets were combined after  
680 aggregating relative abundances at the bacterial order taxonomic level. The core taxa of the root  
681 microbiota were determined by identifying bacterial orders present in every plant species with an  
682 occupancy of at least 80% (i.e., found in at least 80% of the root samples of a given species) with  
683 a relative abundance above 0.1%. To infer the phylogenetic relationship between the different  
684 hosts, protein sequences of the ribulose-bisphosphate carboxylase (*rbcL*) gene for *Cr* and the 35  
685 analyzed plant species were recovered from GenBank. The sequences were aligned using Clustal  
686 Omega (Sievers *et al.*, 2011) with default parameters, and the alignment used to infer a maximum  
687 likelihood phylogeny using FastTree (Price *et al.*, 2010).

### 688 **Analysis of culture-dependent amplicon sequencing data**

689 Sequencing data from SynCom experiments was pre-processed similarly as natural community  
690 16S rRNA data. Quality-filtered, merged paired-end reads were then aligned to a reference set of  
691 sequences extracted from the whole-genome assemblies of every strain included in a given  
692 SynCom, using Rbec (Zhang *et al.*, 2021b). We then checked that the fraction of unmapped reads  
693 did not significantly differ between compartment, experiment or host species. Next, we generated



694 a count table that was employed for downstream analyses of diversity with the R package *vegan*.  
695 Finally, we visualized amplicon data from all experimental systems using the *ggplot2* R package  
696 ([Wickham et al., 2016](#)).

## 697 **Genome assembly and annotation**

698 Paired-end Illumina reads were first trimmed and quality-filtered using Trimmomatic ([Bolger et al.,](#)  
699 [2014](#)). QC reads were assembled using the IDBA assembler ([Peng et al., 2012](#)) within the A5  
700 pipeline ([Tritt et al., 2012](#)). Assembly statistics and metadata from the assembled genomes can  
701 be found in **Supplementary Data 3**. Genome assemblies with either multi-modal *k*-mer and G+C  
702 content distributions or multiple cases of marker genes from diverse taxonomic groups were  
703 flagged as not originating from clonal cultures. Such assemblies were then processed using a  
704 metagenome binning approach ([Pasolli et al., 2019](#)). Briefly, contigs from each of these samples  
705 were clustered using METABAT2 ([Kang et al., 2019](#)) to obtain metagenome-assembled genomes  
706 (MAGs). Each MAG was analyzed to assess completeness and contamination using CheckM  
707 ([Parks et al., 2015](#)). Only bins with completeness scores larger than 75% and contamination rates  
708 lower than 5% were retained and added to the collection (**Supplementary Data 3**; designated  
709 MAG in the column 'type'). Classification of the bacterial genomes into phylogroups was performed  
710 by calculating pair-wise average nucleotide identities using FastANI ([Jain et al., 2018](#)) and  
711 clustering at a 97% similarity threshold. Functional annotation of the genomes was conducted  
712 using Prokka ([Seeman et al., 2014](#)) with a custom database based on KEGG Orthologue (KO)  
713 groups ([Kanehisa et al., 2014](#)) downloaded from the KEGG FTP server in November 2019. Hits  
714 to sequences in the database were filtered using an *E*-value threshold of  $10 \times 10^{-9}$  and a minimum  
715 coverage of 80% of the length of the query sequence.

## 716 **Comparative genome analyses of the *Cr*-, *At*- and *Lj*-SPHERE culture collections**

717 The genomes from the *Cr*-, *At*- and *Lj*-SPHERE culture collections ([Bai et al., 2015](#); [Wippel et al.,](#)  
718 [2021](#)) were queried for the presence of 31 conserved, single-copy marker genes, known as  
719 AMPHORA genes ([Wu et al., 2008](#)). Next, sequences of each gene were aligned using Clustal  
720 Omega ([Sievers et al., 2011](#)) with default parameters. Using a concatenated alignment of each  
721 gene, we inferred a maximum likelihood phylogeny using FastTree ([Price et al., 2010](#)). This tree  
722 was visualized using the Interactive Tree of Life web tool ([Letunic et al., 2019](#)). Finally, genomes  
723 from the three collections (*Cr*-SPHERE, *At*-SPHERE and *Lj*-SPHERE) were clustered into  
724 phylogroups, roughly corresponding to a species designation ([Olm et al., 2020](#)) using FastANI  
725 ([Jain et al., 2018](#)) and a threshold of average nucleotide identity at the whole genome level of at  
726 least 97%. Functional comparison among the genomes from the *Cr*-, *Lj*- and *At*-SPHERE

727 collections was performed by comparing their annotations. KO groups were gathered from the  
728 genome annotations and aggregated into a single table. Lastly, functional distances between  
729 genomes based on Pearson correlations were used for principal coordinate analysis using the  
730 *cmdscale* function in R.

### 731 **Data deposition**

732 Raw sequencing will be deposited into the European Nucleotide Archive (ENA) under the  
733 accession number PRJEB43117. The scripts used for the computational analyses described in  
734 this study are available at <http://www.github.com/garridoo/crsphere>, to ensure replicability and  
735 reproducibility of these results.

### 736 **Author contributions**

737 P.D., J.F.-U., K.W. and R.G.-O. designed the experiments. P.D. and J.F.-U. conducted the  
738 greenhouse experiments. P.D. and K.W. performed the mesocosm experiments. P.D., J.F.-U.,  
739 and K.W. established the IPL bacterial library and characterized the *Cr*-SPHERE core culture  
740 collection. P.D. and J.F.-U. performed the synthetic community experiments. P.Z., J.F.-U. and  
741 R.G.-O. analyzed whole-genome sequencing data. P.D., J.F.-U., P.Z., R.G. and R.G.-O. analyzed  
742 bacterial 16S rRNA amplicon data. P.D., J.F.-U., K.W. and R.G.-O interpreted the results. P.D.,  
743 J.F.-U. and R.G.-O wrote the paper.

### 744 **Acknowledgements**

745 We would like to thank Dr. Paul Schulze-Lefert for his support and advice throughout the duration  
746 of this project. We would also like to thank Dr. Michael Melkonian, Dr. Stephane Hacquard, Dr.  
747 Thomas Nakano, Dr. Oliver Ebenhöf, and Dr. Andreas Weber for their critical comments on this  
748 manuscript. We thank Dr. Ralph Bock, Dr. Juliane Neupert and Dr. Ru Zhang for their advice and  
749 assistance during the early stages of this research project. Finally, we thank Rozina Kardarakis  
750 for grammatical and style corrections of the manuscript. This research was funded by the Max  
751 Planck Society and the Deutsche Forschungsgemeinschaft (DFG, German Research Foundation)  
752 under Germany's Excellence Strategy – EXC-Nummer 2048/1– project 390686111, and the '2125  
753 DECrypT' Priority Programme.

754 **References**

- 755 Alcaraz, L.D., Peimbert, M., Barajas, H.R., Dorantes-Acosta, A.E., Bowman, J.L., and Arteaga-  
756 Vázquez, M.A. (2018). Marchantia liverworts as a proxy to plants' basal microbiomes. *Sci. Rep.*  
757 *8*, 1–12.
- 758 Alvarez, L., Aliashkevich, A., De Pedro, M.A., and Cava, F. (2018). Bacterial secretion of D-  
759 arginine controls environmental microbial biodiversity. *ISME J.* *12*, 438–450.
- 760 Amin, S.A., Hmelo, L.R., Van Tol, H.M., Durham, B.P., Carlson, L.T., Heal, K.R., Morales, R.L.,  
761 Berthiaume, C.T., Parker, M.S., Djunaedi, B., et al. (2015). Interaction and signalling between a  
762 cosmopolitan phytoplankton and associated bacteria. *Nature* *522*, 98–101.
- 763 Amin, S.A., Green, D.H., Hart, M.C., Küpper, F.C., Sunda, W.G., and Carrano, C.J. (2009).  
764 Photolysis of iron-siderophore chelates promotes bacterial-algal mutualism. *Proc. Natl. Acad. Sci.*  
765 *U. S. A.* *106*, 17071–17076.
- 766 Bai, Y., Müller, D.B., Srinivas, G., Garrido-Oter, R., Potthoff, E., Rott, M., Dombrowski, N., Münch,  
767 P.C., Spaepen, S., Remus-Emsermann, M., et al. (2015). Functional overlap of the Arabidopsis  
768 leaf and root microbiota. *Nature* *528*, 364–369.
- 769 Baudoin, E., Benizri, E., and Guckert, A. (2003). Impact of artificial root exudates on the bacterial  
770 community structure in bulk soil and maize rhizosphere. *Soil Biol. Biochem.* *35*, 1183–1192.
- 771 Beckers, B., De Beeck, M.O., Weyens, N., Boerjan, W., and Vangronsveld, J. (2017). Structural  
772 variability and niche differentiation in the rhizosphere and endosphere bacterial microbiome of  
773 field-grown poplar trees. *Microbiome* *5*, 1–17.
- 774 Bell, W., and Mitchell, R. (1972). Chemotactic and growth responses of marine bacteria to algal  
775 extracellular products. *Biol. Bull.* *143*, 265–277.
- 776 Berens, M.L., Wolinska, K.W., Spaepen, S., Ziegler, J., Nobori, T., Nair, A., Krüler, V.,  
777 Winkelmüller, T.M., Wang, Y., Mine, A., et al. (2019). Balancing trade-offs between biotic and  
778 abiotic stress responses through leaf age-dependent variation in stress hormone cross-talk. *Proc.*  
779 *Natl. Acad. Sci. U. S. A.* *116*, 2364–2373.
- 780 Bolger, A.M., Lohse, M., and Usadel, B. (2014). Trimmomatic: a flexible trimmer for Illumina  
781 sequence data. *Bioinformatics* *30*, 2114–2120.
- 782 Broughton, W.J., and Dilworth, M.J. (1971). Control of leghaemoglobin synthesis in snake beans.  
783 *Biochem. J.* *125*, 1075–1080.

- 784 Bulgarelli, D., Garrido-Oter, R., Münch, P.C., Weiman, A., Dröge, J., Pan, Y., McHardy, A.C., and  
785 Schulze-Lefert, P. (2015). Structure and function of the bacterial root microbiota in wild and  
786 domesticated barley. *Cell Host Microbe* 17, 392–403.
- 787 Bulgarelli, D., Rott, M., Schlaeppli, K., Ver Loren van Themaat, E., Ahmadinejad, N., Assenza, F.,  
788 Rauf, P., Huettel, B., Reinhardt, R., Schmelzer, E., et al. (2012). Revealing structure and assembly  
789 cues for *Arabidopsis* root-inhabiting bacterial microbiota. *Nature* 488, 91–95.
- 790 Bulgarelli, D., Schlaeppli, K., Spaepen, S., van Themaat, E.V.L., and Schulze-Lefert, P. (2013).  
791 Structure and Functions of the Bacterial Microbiota of Plants. *Annu. Rev. Plant Biol.* 64, 807–838.
- 792 Callahan, B.J., McMurdie, P.J., Rosen, M.J., Han, A.W., Johnson, A.J.A., and Holmes, S.P.  
793 (2016). DADA2: High-resolution sample inference from Illumina amplicon data. *Nat. Methods* 13,  
794 581–583.
- 795 Caporaso, J.G., Kuczynski, J., Stombaugh, J., Bittinger, K., Bushman, F.D., Costello, E.K., Fierer,  
796 N., Pěa, A.G., Goodrich, J.K., Gordon, J.I., et al. (2010). QIIME allows analysis of high-throughput  
797 community sequencing data. *Nat. Methods* 7, 335–336.
- 798 Carrión, V.J., Perez-Jaramillo, J., Cordovez, V., Tracanna, V., De Hollander, M., Ruiz-Buck, D.,  
799 Mendes, L.W., van Ijcken, W.F.J., Gomez-Exposito, R., Elsayed, S.S., et al. (2019). Pathogen-  
800 induced activation of disease-suppressive functions in the endophytic root microbiome. *Science*  
801 366, 606–612.
- 802 Castrillo, G., Teixeira, P.J.P.L., Paredes, S.H., Law, T.F., De Lorenzo, L., Feltcher, M.E., Finkel,  
803 O.M., Breakfield, N.W., Mieczkowski, P., Jones, C.D., et al. (2017). Root microbiota drive direct  
804 integration of phosphate stress and immunity. *Nature* 543, 513–518.
- 805 Chaparro, J.M., Badri, D. V., Bakker, M.G., Sugiyama, A., Manter, D.K., and Vivanco, J.M. (2013).  
806 Root Exudation of Phytochemicals in *Arabidopsis* Follows Specific Patterns That Are  
807 Developmentally Programmed and Correlate with Soil Microbial Functions. *PLoS One* 8, e55731.
- 808 Cirri, E., and Pohnert, G. (2019). Algae–bacteria interactions that balance the planktonic  
809 microbiome. *New Phytol.* 223, 100–106.
- 810 Cregger, M.A., Veach, A.M., Yang, Z.K., Crouch, M.J., Vilgalys, R., Tuskan, G.A., and Schadt,  
811 C.W. (2018). The *Populus* holobiont: Dissecting the effects of plant niches and genotype on the  
812 microbiome. *Microbiome* 6, 31.
- 813 Croft, M.T., Lawrence, A.D., Raux-Deery, E., Warren, M.J., and Smith, A.G. (2005). Algae acquire  
814 vitamin B12 through a symbiotic relationship with bacteria. *Nature* 438, 90–93.

- 815 de Zélicourt, A., Synek, L., Saad, M.M., Alzubaidy, H., Jalal, R., Xie, Y., Andrés-Barrao, C., Rolli,  
816 E., Guerard, F., Mariappan, K.G., et al. (2018). Ethylene induced plant stress tolerance by  
817 *Enterobacter* sp. SA187 is mediated by 2-keto-4-methylthiobutyric acid production. *PLoS Genet.*  
818 *14*, e1007273.
- 819 Delaux, P.M., Radhakrishnan, G. V., Jayaraman, D., Cheema, J., Malbreil, M., Volkening, J.D.,  
820 Sekimoto, H., Nishiyama, T., Melkonian, M., Pokorny, L., et al. (2015). Algal ancestor of land  
821 plants was preadapted for symbiosis. *Proc. Natl. Acad. Sci. U. S. A.* *112*, 13390–13395.
- 822 Demoling, F., Figueroa, D., and Bååth, E. (2007). Comparison of factors limiting bacterial growth  
823 in different soils. *Soil Biol. Biochem.* *39*, 2485–2495.
- 824 Durán, P., Thiergart, T., Garrido-Oter, R., Agler, M., Kemen, E., Schulze-Lefert, P., and Hacquard,  
825 S. (2018). Microbial Interkingdom Interactions in Roots Promote Arabidopsis Survival. *Cell* *175*,  
826 973-983.e14.
- 827 Edgar, R.C. (2010). Search and clustering orders of magnitude faster than BLAST. *Bioinformatics*  
828 *26*, 2460–2461.
- 829 Edgar, R.C. (2013). UPARSE: Highly accurate OTU sequences from microbial amplicon reads.  
830 *Nat. Methods* *10*, 996–998.
- 831 Edgar, R.C., Haas, B.J., Clemente, J.C., Quince, C., and Knight, R. (2011). UCHIME improves  
832 sensitivity and speed of chimera detection. *Bioinformatics* *27*, 2194–2200.
- 833 Edwards, J., Johnson, C., Santos-Medellín, C., Lurie, E., Podishetty, N.K., Bhatnagar, S., Eisen,  
834 J.A., Sundaresan, V., and Jeffery, L.D. (2015). Structure, variation, and assembly of the root-  
835 associated microbiomes of rice. *Proc. Natl. Acad. Sci. U. S. A.* *112*, E911–E920.
- 836 Eida, A.A., Ziegler, M., Lafi, F.F., Michell, C.T., Voolstra, C.R., Hirt, H., and Saad, M.M. (2018).  
837 Desert plant bacteria reveal host influence and beneficial plant growth properties. *PLoS One* *13*,  
838 e0208223.
- 839 Fu, H., Uchimiya, M., Gore, J., and Moran, M.A. (2020). Ecological drivers of bacterial community  
840 assembly in synthetic phycospheres. *Proc. Natl. Acad. Sci. U. S. A.* *117*, 3656–3662.
- 841 Garrido-Oter, R., Nakano, R.T., Dombrowski, N., Ma, K.W., McHardy, A.C., and Schulze-Lefert,  
842 P. (2018). Modular Traits of the Rhizobiales Root Microbiota and Their Evolutionary Relationship  
843 with Symbiotic Rhizobia. *Cell Host Microbe* *24*, 155-167.e5.

- 844 Grant, M.A.A., Kazamia, E., Cicuta, P., and Smith, A.G. (2014). Direct exchange of vitamin B 12  
845 is demonstrated by modelling the growth dynamics of algal-bacterial cocultures. *ISME J.* 8, 1418–  
846 1427.
- 847 Harbort, C.J., Hashimoto, M., Inoue, H., Niu, Y., Guan, R., Rombolà, A.D., Kopriva, S., Voges,  
848 M.J.E.E.E., Sattely, E.S., Garrido-Oter, R., et al. (2020). Root-Secreted Coumarins and the  
849 Microbiota Interact to Improve Iron Nutrition in Arabidopsis. *Cell Host Microbe* 28, 825-837.e6.
- 850 Harris, E. H. (2009). *The Chlamydomonas Sourcebook*. - 2. ed. (San Diego: Academic Press)
- 851 Horňák, K., Kasalický, V., Šimek, K., and Grossart, H.-P. (2017). Strain-specific consumption and  
852 transformation of alga-derived dissolved organic matter by members of the *Limnohabitans* -C and  
853 *Polynucleobacter* -B clusters of *Betaproteobacteria*. *Environ. Microbiol.* 19, 4519–4535.
- 854 Huang, A.C., Jiang, T., Liu, Y.X., Bai, Y.C., Reed, J., Qu, B., Goossens, A., Nützmann, H.W., Bai,  
855 Y., and Osbourn, A. (2019). A specialized metabolic network selectively modulates Arabidopsis  
856 root microbiota. *Science* 364, eaau6389.
- 857 Jain, C., Rodriguez-R, L.M., Phillippy, A.M., Konstantinidis, K.T., and Aluru, S. (2018). High  
858 throughput ANI analysis of 90K prokaryotic genomes reveals clear species boundaries. *Nat.*  
859 *Commun.* 9, 1–8.
- 860 Kanehisa, M., Goto, S., Sato, Y., Kawashima, M., Furumichi, M., and Tanabe, M. (2014). Data,  
861 information, knowledge and principle: Back to metabolism in KEGG. *Nucleic Acids Res.* 42, D199–  
862 D205.
- 863 Kang, D.D., Li, F., Kirton, E., Thomas, A., Egan, R., An, H., and Wang, Z. (2019). MetaBAT 2: an  
864 adaptive binning algorithm for robust and efficient genome reconstruction from metagenome  
865 assemblies. *PeerJ* 7, e7359.
- 866 Karasov, T.L., Almario, J., Friedemann, C., Ding, W., Giolai, M., Heavens, D., Kersten, S.,  
867 Lundberg, D.S., Neumann, M., Regalado, J., et al. (2018). Arabidopsis thaliana and Pseudomonas  
868 Pathogens Exhibit Stable Associations over Evolutionary Timescales. *Cell Host Microbe* 24, 168-  
869 179.e4.
- 870 Kim, B.H., Ramanan, R., Cho, D.H., Oh, H.M., and Kim, H.S. (2014). Role of Rhizobium, a plant  
871 growth promoting bacterium, in enhancing algal biomass through mutualistic interaction. *Biomass*  
872 *and Bioenergy* 69, 95–105.



- 873 Kim, B.H., Ramanan, R., Cho, D.H., Oh, H.M., and Kim, H.S. (2014). Role of Rhizobium, a plant  
874 growth promoting bacterium, in enhancing algal biomass through mutualistic interaction. *Biomass*  
875 and *Bioenergy* 69, 95–105.
- 876 Knack, J.J., Wilcox, L.W., Delaux, P.-M., Ané, J.-M., Piotrowski, M.J., Cook, M.E., Graham, J.M.,  
877 and Graham, L.E. (2015). Microbiomes of Streptophyte Algae and Bryophytes Suggest That a  
878 Functional Suite of Microbiota Fostered Plant Colonization of Land. *Int. J. Plant Sci.* 176, 405–  
879 420.
- 880 Kremer, J. M., Sohrabi, R., Paasch, B. C., Rhodes, D., Thireault, C., Schulze-Lefert, P., Tiedje,  
881 J. M., He, S. Y. (2021) Peat-based gnotobiotic plant growth systems for Arabidopsis microbiome  
882 research. *Nature Protocols*, in press.
- 883 Krohn-Molt, I., Alawi, M., Förstner, K.U., Wiegandt, A., Burkhardt, L., Indenbirken, D., Thieß, M.,  
884 Grundhoff, A., Kehr, J., Tholey, A., et al. (2017). Insights into Microalga and Bacteria Interactions  
885 of Selected Phycosphere Biofilms Using Metagenomic, Transcriptomic, and Proteomic  
886 Approaches. *Front. Microbiol.* 8, 1941.
- 887 Kropat, J., Hong-Hermesdorf, A., Casero, D., Ent, P., Castruita, M., Pellegrini, M., Merchant, S.S.,  
888 and Malasarn, D. (2011). A revised mineral nutrient supplement increases biomass and growth  
889 rate in *Chlamydomonas reinhardtii*. *Plant J.* 66, 770–780.
- 890 Lebeis, S.L., Paredes, S.H., Lundberg, D.S., Breakfield, N., Gehring, J., McDonald, M., Malfatti,  
891 S., Del Rio, T.G., Jones, C.D., Tringe, S.G., et al. (2015). Salicylic acid modulates colonization of  
892 the root microbiome by specific bacterial taxa. *Science* 349, 860–864.
- 893 Letunic, I., and Bork, P. (2019). Interactive Tree of Life (iTOL) v4: Recent updates and new  
894 developments. *Nucleic Acids Res.* 47, W256–W259.
- 895 Lundberg, D.S., Lebeis, S.L., Paredes, S.H., Yourstone, S., Gehring, J., Malfatti, S., Tremblay, J.,  
896 Engelbrekton, A., Kunin, V., Rio, T.G. Del, et al. (2012). Defining the core *Arabidopsis thaliana*  
897 root microbiome. *Nature* 488, 86–90.
- 898 Moran, M.A., Kujawinski, E.B., Stubbins, A., Fatland, R., Aluwihare, L.I., Buchan, A., Crump, B.C.,  
899 Dorrestein, P.C., Dyrman, S.T., Hess, N.J., et al. (2016). Deciphering ocean carbon in a changing  
900 world. *Proc. Natl. Acad. Sci. U. S. A.* 113, 3143–3151.
- 901 Oksanen, J., Blanchet, F.G., Friendly, M., Kindt, R., Legendre, P., Mcglinn, D., Minchin, P.R.,  
902 O'Hara, R.B., Simpson, G.L., Solymos, P., et al. (2019). *vegan: Community Ecology Package*. R  
903 package version 2.4-2.

- 904 Olm, M.R., Crits-Christoph, A., Diamond, S., Lavy, A., Matheus Carnevali, P.B., and Banfield, J.F.  
905 (2020). Consistent Metagenome-Derived Metrics Verify and Delineate Bacterial Species  
906 Boundaries. *MSystems* 5.
- 907 Paerl, R.W., Bouget, F.Y., Lozano, J.C., Vergé, V., Schatt, P., Allen, E.E., Palenik, B., and Azam,  
908 F. (2017). Use of plankton-derived vitamin B1 precursors, especially thiazole-related precursor,  
909 by key marine picoeukaryotic phytoplankton. *ISME J.* 11, 753–765.
- 910 Parks, D.H., Imelfort, M., Skennerton, C.T., Hugenholtz, P., and Tyson, G.W. (2015). CheckM:  
911 assessing the quality of microbial genomes recovered from isolates, single cells, and  
912 metagenomes. *Genome Res.* 25, 1043–1055.
- 913 Pasolli, E., Asnicar, F., Manara, S., Zolfo, M., Karcher, N., Armanini, F., Beghini, F., Manghi, P.,  
914 Tett, A., Ghensi, P., et al. (2019). Extensive Unexplored Human Microbiome Diversity Revealed  
915 by Over 150,000 Genomes from Metagenomes Spanning Age, Geography, and Lifestyle. *Cell*  
916 176, 649-662.e20.
- 917 Peng, Y., Leung, H.C.M., Yiu, S.M., and Chin, F.Y.L. (2012). IDBA-UD: a de novo assembler for  
918 single-cell and metagenomic sequencing data with highly uneven depth. *Bioinformatics* 28, 1420–  
919 1428.
- 920 Porra, R.J., Thompson, W.A., and Kriedemann, P.E. (1989). Determination of accurate extinction  
921 coefficients and simultaneous equations for assaying chlorophylls a and b extracted with four  
922 different solvents: verification of the concentration of chlorophyll standards by atomic absorption  
923 spectroscopy. *BBA - Bioenerg.* 975, 384–394.
- 924 Price, M.N., Dehal, P.S., and Arkin, A.P. (2010). FastTree 2 - Approximately maximum-likelihood  
925 trees for large alignments. *PLoS One* 5, e9490.
- 926 Quast, C., Pruesse, E., Yilmaz, P., Gerken, J., Schweer, T., Yarza, P., Peplies, J., and Glöckner,  
927 F.O. (2013). The SILVA ribosomal RNA gene database project: Improved data processing and  
928 web-based tools. *Nucleic Acids Res.* 41, D590–D596.
- 929 Sasso, S., Stibor, H., Mittag, M., and Grossman, A.R. (2018). The natural history of model  
930 organisms from molecular manipulation of domesticated *chlamydomonas reinhardtii* to survival in  
931 nature. *Elife* 7.
- 932 Schlaeppi, K., Dombrowski, N., Oter, R.G., Ver Loren Van Themaat, E., and Schulze-Lefert, P.  
933 (2014). Quantitative divergence of the bacterial root microbiota in *Arabidopsis thaliana* relatives.  
934 *Proc. Natl. Acad. Sci. U. S. A.* 111, 585–592.

- 935 Seemann, T. (2014). Prokka: rapid prokaryotic genome annotation. *Bioinformatics* 30, 2068–2069.
- 936 Seymour, J.R., Amin, S.A., Raina, J.-B., and Stocker, R. (2017). Zooming in on the phycosphere:  
937 the ecological interface for phytoplankton–bacteria relationships. *Nat. Microbiol.* 2, 17065.
- 938 Shibl, A.A., Isaac, A., Ochsenkühn, M.A., Cárdenas, A., Fei, C., Behringer, G., Arnoux, M., Drou,  
939 N., Santos, M.P., Gunsalus, K.C., et al. (2020). Diatom modulation of select bacteria through use  
940 of two unique secondary metabolites. *Proc. Natl. Acad. Sci.* 117, 27445–27455.
- 941 Sievers, F., Wilm, A., Dineen, D., Gibson, T.J., Karplus, K., Li, W., Lopez, R., McWilliam, H.,  
942 Remmert, M., Söding, J., et al. (2011). Fast, scalable generation of high-quality protein multiple  
943 sequence alignments using Clustal Omega. *Mol. Syst. Biol.* 7, 539.
- 944 Simmons, T., Styer, A.B., Pierroz, G., Gonçalves, A.P., Pasricha, R., Hazra, A.B., Bubner, P., and  
945 Coleman-Derr, D. (2020). Drought Drives Spatial Variation in the Millet Root Microbiome. *Front.*  
946 *Plant Sci.* 11, 599.
- 947 Smriga, S., Fernandez, V.I., Mitchell, J.G., and Stocker, R. (2016). Chemotaxis toward  
948 phytoplankton drives organic matter partitioning among marine bacteria. *Proc. Natl. Acad. Sci. U.*  
949 *S. A.* 113, 1576–1581.
- 950 Suárez-Moreno, Z.R., Caballero-Mellado, J., Coutinho, B.G., Mendonça-Previato, L., James, E.K.,  
951 and Venturi, V. (2012). Common Features of Environmental and Potentially Beneficial Plant-  
952 Associated Burkholderia. *Microb. Ecol.* 63, 249–266.
- 953 Teplitski, M., Chen, H., Rajamani, S., Gao, M., Merighi, M., Sayre, R.T., Robinson, J.B., Rolfe,  
954 B.G., and Bauer, W.D. (2004). *Chlamydomonas reinhardtii* Secretes Compounds That Mimic  
955 Bacterial Signals and Interfere with Quorum Sensing Regulation in Bacteria. *Plant Physiol.* 134,  
956 137–146.
- 957 Thiergart, T., Zgadzaj, R., Bozsóki, Z., Garrido-Oter, R., Radutoiu, S., and Schulze-Lefert, P.  
958 (2019). *Lotus japonicus* symbiosis genes impact microbial interactions between symbionts and  
959 multikingdom commensal communities. *MBio* 10, 1833–1852.
- 960 Thiergart, T., Durán, P., Ellis, T., Vannier, N., Garrido-Oter, R., Kemen, E., Roux, F., Alonso-  
961 Blanco, C., Ågren, J., Schulze-Lefert, P., et al. (2020). Root microbiota assembly and adaptive  
962 differentiation among European *Arabidopsis* populations. *Nat. Ecol. Evol.* 4, 122–131.
- 963 Timilsina, S., Potnis, N., Newberry, E.A., Liyanapathirana, P., Iruegas-Bocardo, F., White, F.F.,  
964 Goss, E.M., and Jones, J.B. (2020). *Xanthomonas* diversity, virulence and plant–pathogen  
965 interactions. *Nat. Rev. Microbiol.* 18, 415–427.

- 966 Toyama, T., Kasuya, M., Hanaoka, T., Kobayashi, N., Tanaka, Y., Inoue, D., Sei, K., Morikawa,  
967 M., and Mori, K. (2018). Growth promotion of three microalgae, *Chlamydomonas reinhardtii*,  
968 *Chlorella vulgaris* and *Euglena gracilis*, by in situ indigenous bacteria in wastewater effluent.  
969 *Biotechnol. Biofuels* 11, 176.
- 970 Tritt, A., Eisen, J.A., Facciotti, M.T., and Darling, A.E. (2012). An Integrated Pipeline for de Novo  
971 Assembly of Microbial Genomes. *PLoS One* 7, e42304.
- 972 Walters, W.A., Jin, Z., Youngblut, N., Wallace, J.G., Sutter, J., Zhang, W., González-Peña, A.,  
973 Peiffer, J., Koren, O., Shi, Q., et al. (2018). Large-scale replicated field study of maize rhizosphere  
974 identifies heritable microbes. *Proc. Natl. Acad. Sci. U. S. A.* 115, 7368–7373.
- 975 Wichard, T., Charrier, B., Mineur, F., Bothwell, J.H., Clerck, O. De, and Coates, J.C. (2015). The  
976 green seaweed *Ulva*: a model system to study morphogenesis. *Front. Plant Sci.* 6, 72.
- 977 Wickham, H. (2016). *ggplot2* (Cham: Springer International Publishing).
- 978 Wienhausen, G., Noriega-Ortega, B.E., Niggemann, J., Dittmar, T., and Simon, M. (2017). The  
979 exometabolome of two model strains of the *Roseobacter* group: A marketplace of microbial  
980 metabolites. *Front. Microbiol.* 8, 1985.
- 981 Wippel, K., Tao, K., Niu, Y., Zgadzaj, R., Guan, R., Dahms, E., Jensen, D.B., Logemann, E.,  
982 Radutoiu, S., Schulze-Lefert, P., et al. (2021). Host preference and invasiveness of commensals  
983 in the *Lotus* and *Arabidopsis* root microbiota. *BioRxiv*, 10.1101/2021.01.12.426357.
- 984 Wu, M., and Eisen, J.A. (2008). A simple, fast, and accurate method of phylogenomic inference.  
985 *Genome Biol.* 9, 1–11.
- 986 Xu, L., Naylor, D., Dong, Z., Simmons, T., Pierroz, G., Hixson, K.K., Kim, Y.M., Zink, E.M.,  
987 Engbrecht, K.M., Wang, Y., et al. (2018). Drought delays development of the sorghum root  
988 microbiome and enriches for monoderm bacteria. *Proc. Natl. Acad. Sci. U. S. A.* 115, E4284–  
989 E4293.
- 990 Yeoh, Y.K., Dennis, P.G., Paungfoo-Lonhienne, C., Weber, L., Brackin, R., Ragan, M.A., Schmidt,  
991 S., and Hugenholtz, P. (2017). Evolutionary conservation of a core root microbiome across plant  
992 phyla along a tropical soil chronosequence. *Nat. Commun.* 8, 1–9.
- 993 Zgadzaj, R., Garrido-Oter, R., Jensen, D.B., Koprivova, A., Schulze-Lefert, P., and Radutoiu, S.  
994 (2016). Root nodule symbiosis in *Lotus japonicus* drives the establishment of distinctive  
995 rhizosphere, root, and nodule bacterial communities. *Proc. Natl. Acad. Sci. U. S. A.* 113, E7996–  
996 E8005.

- 997 Zhalnina, K., Louie, K.B., Hao, Z., Mansoori, N., Da Rocha, U.N., Shi, S., Cho, H., Karaoz, U.,  
998 Loqué, D., Bowen, B.P., et al. (2018). Dynamic root exudate chemistry and microbial substrate  
999 preferences drive patterns in rhizosphere microbial community assembly. *Nat. Microbiol.* 3, 470–  
1000 480.
- 1001 Zhang, J., Liu, Y.X., Zhang, N., Hu, B., Jin, T., Xu, H., Qin, Y., Yan, P., Zhang, X., Guo, X., et al.  
1002 (2019). NRT1.1B is associated with root microbiota composition and nitrogen use in field-grown  
1003 rice. *Nat. Biotechnol.* 37, 676–684.
- 1004 Zhang, J., Liu, Y.-X., Guo, X., Qin, Y., Garrido-Oter, R., Schulze-Lefert, P., and Bai, Y. (2021a).  
1005 High-throughput cultivation and identification of bacteria from the plant root microbiota. *Nat.*  
1006 *Protoc.* 16, 988–1012.
- 1007 Zhang, P., Spaepen, S., Bai, Y., Hacquard, S., and Garrido-Oter, R. (2021b). Reference-based  
1008 error correction of amplicon sequencing data from synthetic communities.  
1009 *BioRxiv*, 10.1101/2021.01.15.426834.